JOURNAL OF COMPUTATIONAL PHYSICS 35, 110–145 (1980)

Nonlinear, Two-Dimensional Magnetohydrodynamic Calculations*

D. SCHNACK AND J. KILLEEN

National Magnetic Fusion Energy Computer Center, Lawrence Livermore Laboratory, Livermore, California 94550, and Department of Applied Science, University of California, Davis/Livermore, Livermore, California 94550

Received, November 7, 1978; revised, March 27, 1979

A nonlinear, time-dependent, hydromagnetic model is developed. The model is based on the eight partial differential equations of resistive magnetohydrodynamics (MHD). The equations are expressed as a set of conservation laws which are written in general, orthogonal, curvilinear coordinates in two space dimensions. No assumption about the ordering of terms is made. The resulting equations are then solved by the method of finite differences on an Eulerian mesh. We develop spatial finite-difference techniques which guarantee the simultaneous conservation of the desired physical quantities throughout the course of the calculation. Conservative boundary conditions on thermodynamic quantities at a conducting boundary are derived, and special algorithms are developed for advancing the solution at a singular boundary. For the temporal differencing, we use the Alternating Direction Implicit (ADI) method. We apply our model to the difficult case of resistive instabilities. We present results relevant to the nonlinear evolution of these modes in three distinct coordinate systems. One of these cases depends on finite plasma pressure, and can be studied only with a general model such as that presented here.

1. INTRODUCTION

With the advances in speed and memory size of modern computers, it has become feasible to study plasma instabilities by numerical techniques. For the case of ideal (infinitely conducting) magnetohydrodynamics (MHD), computations of the linear behavior of these modes have followed two paths: calculations based on the energy principle [1, 2], which have yielded significant information about the spectrum of ideal MHD activity in plasmas; and calculations based on the solution of an initial-value problem in which the linearized fluid equations are advanced in time until an exponentially growing solution appears [3–6].

In order to study the long-time, large-amplitude behavior of plasma instabilities, and to simulate experimental devices in controlled fusion research, the nonlinear fluid equations must be solved. In general, such a calculation requires the simultaneous advancement in time of eight nonlinear partial differential equations in several spatial dimensions. Early codes of this type are reviewed by Roberts and Potter [7].

* Work performed under the auspices of the U.S. Department of Energy by the Lawrence Livermore Laboratory under Contract W-7405-ENG-48.

0021-9991/80/040110–36$02.00/0

Codes which model the behavior of an infinitely conducting plasma in several spatial dimensions have recently appeared. Brackbill [8] has used a moving computational grid in extensive simulations of the Scyllac experiment. Bateman *et al.* [9] have used explicit methods on an Eulerian mesh to study fixed-boundary MHD instabilities, and recently Jardin *et al.* [10, 11] have introduced dynamical grid methods in their studies of tokamak instabilities. Strauss [12, 13] has used modified equations to study the nonlinear evolution of tokamak plasmas, and Pritchett *et al.* [45] have used an explicit nonlinear code to study the evolution of ideal interchange instabilities.

More realistic modeling of plasma behavior requires that transport coefficients, such as resistivity, be included. Explicit codes in two [14] and three [15–17] spatial dimensions are now in existence. However, the inclusion of resistivity changes the equations from hyperbolic to parabolic, with the result that explicit methods may not be adequate for reasons of economics (computer time) and numerical stability. Lindemuth and Killeen [18] were the first to use implicit finite-difference methods for nonlinear multidimensional MHD problems. Later versions of this code have successfully simulated z-pinch implosions [19] by excluding two components of the magnetic field and one component of the velocity from the model. Lui and Chu [20, 21] have used implicit methods to simulate the implosion phase of cylindrical and belt pinch experiments. Finan [22] is using implicit methods to solve the full set of resistive MHD equations in three space dimensions.

One of the effects of nonvanishing resistivity is the occurrence of unstable modes which have no counterpart in ideal MHD theory [23]. These resistive instabilities grow on time scales which can be long relative to the fastest time scales of the system, leading to severe computational problems. Recently, the evolution and interaction of these modes in tokamaks have been successfully and extensively studied [24–28] by assuming an ordering that eliminates the fastest time scales from the problem, and results in a reduced set of equations for the scalar flux and stream functions [29]. This allows the calculation to proceed rapidly for the large values of magnetic Reynolds number typical of tokamak discharges. However, certain effects, such as those due to finite plasma pressure, are excluded. These effects can be important in controlled fusion devices, such as Reversed Field Pinches and High Beta Tokamaks, which expect to operate with nonvanishing values of $\beta = p/B^2$.

In this paper we describe a two-dimensional, nonlinear, resistive MHD model which retains all the normal modes of the system. It is general in that the equations are cast in orthogonal curvilinear coordinates, making calculations in a variety of coordinate systems possible. For certain cases, the model employs a transformation to helical coordinates which allows the solution of the three-dimensional equations under the assumption that helical symmetry is preserved. Certain phenomena, such as nonlinear coupling of modes of different helicity, are thus not observed.

In Section 2 we present the mathematical model in which the relevant equations are expressed as a set of conservation laws. Computational techniques for the solution of these equations are discussed in Section 3. The question of boundary conditions, including the important case of singular boundaries, is addressed in Section 4. In Section 5 we present examples of the application of our code to resistive instabilities,

an important and difficult case when the diffusive and convective time scales are widely separated. Results are presented in three different coordinate systems. One of our applications involves a mode which depends critically on finite plasma pressure, while the other cases can occur at zero β. These results demonstrate the versatility of the model presented.

2. Mathematical Model

2.1. *Basic Equations*

The equations appropriate for the description of low-frequency, long-wavelength phenomena in a fluid of finite electrical conductivity are the resistive magnetohydrodynamic (MHD) equations. These equations relate the electromagnetic fields **E** and **B** to the fluid velocity **V** and the thermodynamic variables (the pressure p, the mass density ρ, and the specific internal energy e), and may be combined into a set of conservation laws for the magnetic flux density **B**, the fluid momentum density $\rho\mathbf{V}$, the mass density ρ, and the total energy density $u = \rho V^2/2 + B^2/8\pi + \rho e$. In terms of the nondimensional variables

$$\begin{aligned} \mathbf{x}/a &\to \mathbf{x}, & t/t_H &\to t, & \mathbf{B}/B_0 &\to \mathbf{B}, \\ \mathbf{V}/V_A &\to \mathbf{V}, & \rho/\rho_0 &\to \rho, & p/p_0 &\to p, \\ u/u_0 &\to u, & \eta/\eta_0 &\to \eta, \end{aligned}$$

these equations take the form

$$\frac{\partial \mathbf{B}}{\partial t} = \nabla \times \left(\mathbf{V} \times \mathbf{B} - \frac{\eta}{S} \nabla \times \mathbf{B}\right), \tag{2.1a}$$

$$\frac{\partial (\rho \mathbf{V})}{\partial t} = -\nabla \cdot \left[\rho \mathbf{V}\mathbf{V} - \mathbf{B}\mathbf{B} + \frac{1}{2}(p + B^2)\mathbf{I}\right], \tag{2.1b}$$

$$\frac{\partial \rho}{\partial t} = -\nabla \cdot (\rho \mathbf{V}), \tag{2.1c}$$

$$\begin{aligned} \frac{\partial u}{\partial t} = -\nabla \cdot \Big[&(u + p)\mathbf{V} + (B^2\mathbf{I} - 2\mathbf{B}\mathbf{B}) \cdot \mathbf{V} \\ &+ \frac{2\eta}{S}(\mathbf{B} \cdot \nabla \mathbf{B} - \nabla \mathbf{B} \cdot \mathbf{B})\Big], \end{aligned} \tag{2.1d}$$

where η is the electrical resistivity of the fluid, **I** is the unit dyad, and we have assumed Ohm's law in the form $\eta \mathbf{J}/S = \mathbf{E} + \mathbf{V} \times \mathbf{B}$. The pressure is eliminated by assuming

the perfect gas law is valid, so that $\rho e = p/(\gamma - 1)$, where $\gamma = C_p/C_v$ is the ratio of specific heats for the fluid. We can complete the formal transition to conservation form by rewriting (2.1a) as

$$\frac{\partial \mathbf{B}}{\partial t} = \nabla \cdot \left[\mathbf{BV} - \mathbf{VB} + \frac{\eta}{S}(\nabla \mathbf{B} - \nabla \mathbf{B}^{\dagger})\right], \tag{2.1e}$$

where $\nabla \mathbf{B}^{\dagger}$ denote the transpose of the tensor $\nabla \mathbf{B}$. This form will be useful in Section 2.2.

In the normalization described above, subscripts $(\ )_0$ refer to characteristic values of various quantities, a is a characteristic length for changes in the magnetic field, $V_A = B_0/(4\pi\rho_0)^{1/2}$ is the Alfvén velocity, and $t_H = a/V_A$ is the hydromagnetic (or Alfvén) transit time, i.e., the time it would take an Alfvén wave to propagate a distance a. The normalization of the thermodynamic quantities is chosen such that $u_0 = p_0 = B_0^2/8\pi = \rho V_A^2/2$. The quantity $S \equiv t_R/t_H = 4\pi a V_A/c^2\eta_0$ is the magnetic Reynolds number, and measures the ratio of the two characteristic time scales appearing in (2.1): the resistive diffusion time $t_R = 4\pi a^2/c^2\eta_0$, which arises from the term $\nabla \times (\eta \nabla \times \mathbf{B})$; and the Alfvén transit time t_H, defined above, whose origin is the term $\nabla \times (\mathbf{V} \times \mathbf{B})$.

Equations (2.1), along with the equation of state, represent a set of eight nonlinear equations in the eight unknowns $\mathbf{B}$, $\rho\mathbf{V}$, ρ, and u, and constitute the basis of our model.

2.2. *Transformation to Orthogonal Curvilinear Coordinates*

The set of equations (2.1), as written, is valid in any coordinate system. Computationally, we must specify a coordinate system and then expand the indicated vector operations to obtain a set of differential equations to which finite-difference techniques may be applied. In this work we choose to keep these equations as general as possible by specifying the metric as

$$ds^2 = h_1^2 dx_1^2 + h_2^2 dx_2^2 + h_3^2 dx_3^2, \tag{2.2}$$

where x_1, x_2, and x_3 are orthogonal curvilinear coordinates with scale factors $h_i = h_i(x_1, x_2)$.

We now proceed to expand (2.1) in component form. The result is

$$\frac{\partial B^i}{\partial t} = \frac{1}{h_1 h_2 h_3} \frac{\partial}{\partial x^k}(h_1 h_2 h_3 \sigma^{ik}), \tag{2.3a}$$

$$\frac{\partial(\rho V^i)}{\partial t} = \frac{-1}{h_1 h_2 h_3} \frac{\partial}{\partial x^k}(h_1 h_2 h_3 \tau^{ik}) + \tau^{nk} \left\{ \begin{matrix} i \\ nk \end{matrix} \right\}, \tag{2.3b}$$

$$\frac{\partial \rho}{\partial t} = \frac{-1}{h_1 h_2 h_3} \frac{\partial}{\partial x^k} (h_1 h_2 h_3 \rho V^k), \tag{2.3c}$$

$$\frac{\partial u}{\partial t} = \frac{-1}{h_1 h_2 h_3} \frac{\partial}{\partial x^k} (h_1 h_2 h_3 f^k), \tag{2.3d}$$

where σ^{ik} are the contravariant components of the antisymmetric tensor

$$\mathbf{S} = \mathbf{BV} - \mathbf{VB} + (\eta/S)(\nabla \mathbf{B} - \nabla \mathbf{B}^\dagger),$$

τ^{ik} are the contravariant components of the symmetric tensor

$$\mathbf{T} = \rho \mathbf{VV} - \mathbf{BB} + \tfrac{1}{2}(p + B^2)\,\mathbf{I},$$

ρV^k are the contravariant components of the momentum, f^k are the contravariant components of the energy flux

$$\mathbf{F} = (u + p)\,\mathbf{V} + (B^2\mathbf{I} - 2\mathbf{BB}) \cdot \mathbf{V} + (2\eta/S)(\mathbf{B} \cdot \nabla \mathbf{B} - \nabla \mathbf{B} \cdot \mathbf{B}),$$

and we have invoked the summation convention. The Christoffel symbols appearing in (2.3b) arise because of the dependence of the unit vectors on the coordinates, and are defined (with no summation convention) as [30]

$$\left\{ \begin{matrix} i \\ ii \end{matrix} \right\} = \frac{1}{h_i} \frac{\partial h_i}{\partial x^i}, \qquad \left\{ \begin{matrix} i \\ ij \end{matrix} \right\} = \left\{ \begin{matrix} i \\ ji \end{matrix} \right\} = \frac{1}{h_i} \frac{\partial h_i}{\partial x^j},$$

$$\left\{ \begin{matrix} j \\ ii \end{matrix} \right\} = -\frac{h_i}{(h_j)^2} \frac{\partial h_i}{\partial x^j}, \qquad \left\{ \begin{matrix} i \\ jk \end{matrix} \right\} = 0 \quad \text{for } i, j, k \text{ all different.}$$

Even when dependence on x_3 is ignored Eqs. (2.3) are quite complicated, and are tabuled in Appendix A.

Equations (2.3) are the eight equations we solve numerically. The scale factors h_i and their derivatives are specified by function subroutines making any change of coordinate systems a relatively simple matter. In some work we have used an extended set of equations which allow us to solve the full three-dimensional resistive MHD equations under the assumption that certain symmetries are preserved. This is described in the following section.

2.3. *Transformation to Helical Coordinates*

In general, the unstable eigenmodes of a cylindrical plasma are functions of the three spatial dimensions (r, θ, z), and may be written in the form

$$f(r, \theta, z) = \hat{f}_{k_z m}(r)\, e^{i(m\theta + k_z z)} \tag{2.4}$$

where m and k_z are the azimuthal and axial mode numbers, and $\hat{f}_{k_z m}$ is the amplitude of the mode (k_z, m). To describe these cylindrical perturbations in our nonlinear

code, we must reduce the dimensionality of the problem from three to two. This can be done by applying the coordinate transformation

$$\phi = m\theta + k_z z \tag{2.5}$$

to the fully three-dimensional equations. Lines of constant ϕ on a surface of constant radius describe a helix which has the same pitch as the wavefronts of the perturbation (2.4). Such a transformation is clearly an approximation since it does not allow for the nonlinear generation of modes with different helicity; i.e., the original helical symmetry is preserved.

The transformation (2.5) has the effect of adding terms to the flux in the x_2 coordinate direction. For example, a typical conservation law is now written

$$\frac{\partial f}{\partial t} = -\frac{1}{r}\frac{\partial}{\partial r}(rF_r) - \frac{1}{r}\frac{\partial F_\phi}{\partial \phi},$$

where $F_\phi = mF_\theta + rk_zF_z$ is the helical flux of f, i.e., the flux through a helical ribbon with pitch equal to the pitch of the wavefronts of the perturbation. The term proportional to the axial flux F_z does not appear in the formulation (2.3). The equations in this coordinate system have been detailed elsewhere [31, 32].

3. Computational Techniques

3.1. *Conservative Finite-Difference Methods*

Our basic equations form a set of Eulerian conservation laws in the quantities B_1, B_2, B_3, ρV_1, ρV_2, ρV_3, ρ, and u. The scalar conservation laws (2.3c) and (2.3d) conserve total mass and total energy, and the pseudovector conservation law (2.3a) conserves magnetic flux. The vector conservation laws (2.3b) conserve the components of momentum only in coordinate systems in which the scale factors are constants, i.e., Cartesian coordinates. This is because an inertial force (e.g., centrifugal force) is felt by a fluid element which is constrained to move along a path defined by a coordinate which is not a straight line, and we cannot expect to conserve all components of momentum (as referred to the curved coordinate system) in the presence of such a force. (The Cartesian components, however, are always conserved.) The terms responsible for this nonconservation of momentum are called Coriolis terms, and appear as the nonvanishing Christoffel symbols in (2.3b).

When finite-difference approximations are made to the differential operators appearing in our equations it proves convenient to introduce them in such a way that the resulting difference equations have the same conservation properties as the original differential equations. Consider the prototype conservation law

$$\frac{\partial \rho}{\partial t} = -\frac{1}{h_1h_2h_3}\left[\frac{\partial}{\partial x_1}(h_2h_3F) + \frac{\partial}{\partial x_2}(h_1h_3G)\right], \tag{3.1}$$

where ρ is a scalar density and F and G are the x_1 and x_2 fluxes of ρ, respectively. Multiplication of (3.1) by the volume element $d\tau = h_1h_2h_3dx_2dx_2dx_3$ and integration over the allowed range of the independent variables yields the result that the rate of change of the quantity

$$M = \int \rho \, d\tau \tag{3.2}$$

depends only on the values of h_2h_3F and h_1h_3G on the boundaries. We would like our finite-difference approximation to have this same property.

To this end, consider the finite-difference mesh as shown in Fig. 1 with I points in the x_1 direction and J points in the x_2 direction. The coordinates of a given mesh point lie at the center of a cell with vertices $(x_{1_{i-1/2}}, x_{2_{j-1/2}})$, $(x_{1_{i+1/2}}, x_{2_{j-1/2}})$, $(x_{1_{i+1/2}}, x_{2_{j+1/2}})$ and $(x_{1_{i-1/2}}, x_{2_{j+1/2}})$, where $f_{i\pm1/2} \equiv \frac{1}{2}(f_i + f_{i\pm1})$. We then integrate (3.1) over the volume of the cell centered at the mesh point (i,j). We have

$$\begin{aligned}
&\int_{x_{1_{i-1/2}}}^{x_{1_{i+1/2}}} dx_1 \int_{x_{2_{j-1/2}}}^{x_{2_{j+1/2}}} dx_2 \frac{\partial \rho}{\partial t} h_1h_2h_3 \\
&\quad = -\int_{x_{2_{j-1/2}}}^{x_{2_{j+1/2}}} dx_2[(h_2h_3F)_{i+1/2,j} - (h_2h_3F)_{i-1/2,j}] \\
&\quad\quad -\int_{x_{1_{i-1/2}}}^{x_{1_{i+1/2}}} dx_1[(h_1h_3G)_{i,j+1/2} - (h_1h_3G)_{i,j-1/2}].
\end{aligned} \tag{3.3}$$

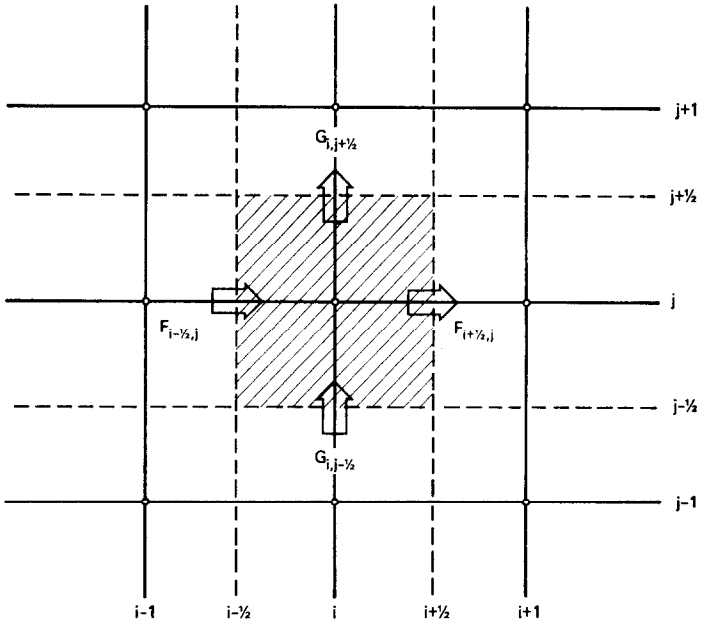

FIG. 1. Computational cell with fluxes defined at cell faces.

We obtain a difference equation by appropriately approximating the integrals in this equation. We use the formulas

$$\int_{x_{i-1/2}}^{x_{i+1/2}} f\,dx = \tfrac{1}{2}f_i(\Delta_+x + \Delta_-x) + O(\Delta x^3), \tag{3.4a}$$

$$\int_{x_{i-1/2}}^{x_{i+1/2}} dx \int_{y_{j-1/2}}^{y_{j+1/2}} dy\, f(x, y) = \tfrac{1}{4}f_{ij}(\Delta_+x + \Delta_-x)(\Delta_+y + \Delta_-y) + O(\Delta x^3) + O(\Delta y^3), \tag{3.4b}$$

where Δ_+ and Δ_- are the forward and backward difference operators at point i, i.e., $\Delta_+x = x_{i+1} - x_i$, $\Delta_-x = x_i - x_{i-1}$. The volume of the cell is

$$\Delta\tau_{ij} = \tfrac{1}{4}(h_1h_2h_3)_{ij}\,(\Delta_+x_1 + \Delta_-x_1)(\Delta_+x_2 + \Delta_-x_2).$$

Then using (3.4) in (3.3), we obtain the spatially discretized equation

$$\frac{\partial\rho_{ij}}{\partial t} = -\frac{2}{(h_1h_2h_3)_{ij}}\left[\frac{(h_2h_3F)_{i+1/2,j} - (h_2h_3F)_{i-1/2,j}}{\Delta_+x_1 + \Delta_-x_1} + \frac{(h_1h_3G)_{i,j+1/2} - (h_1h_3G)_{i,j-1/2}}{\Delta_+x_2 + \Delta_-x_2}\right]. \tag{3.5}$$

The temporal discretization will be discussed in a later section.

We now define the finite-difference analog of Eq. (3.2) as

$$M = \sum_{i=2}^{I-1}\sum_{j=2}^{J-1}\rho_{ij}\,\Delta\tau_{ij}$$

$$= \tfrac{1}{4}\sum_{i=2}^{I-1}\sum_{j=2}^{J-1}\rho_{ij}(h_1h_2h_3)_{ij}(\Delta_+x_1 + \Delta_-x_1)(\Delta_+x_2 + \Delta_-x_2).$$

Then using (3.5), we find

$$\frac{\partial M}{\partial t} = -\sum_{j=2}^{J-1}\frac{(\Delta_+x_2 + \Delta_-x_2)}{2}\left[(h_2h_3F)_{I-1/2,j} - (h_2h_3F)_{3/2,j}\right]$$

$$-\sum_{i=2}^{I-1}\frac{(\Delta_+x_1 + \Delta_-x_1)}{2}\left[(h_1h_3G)_{i,J-1/2} - (h_1h_3G)_{i,3/2}\right],$$

where all the terms in the sums appearing at interior cell boundaries have canceled exactly. Thus, if we choose the points $i = \frac{3}{2}, i = I - \frac{1}{2}, j = \frac{3}{2}, j = J - \frac{1}{2}$ to correspond to solid or periodic boundaries (at $x_1 = x_{1_{\max}}$ and $x_{1_{\min}}$, $x_2 = x_{2_{\max}}$ and $x_{2_{\min}}$), then the quantity M is identically conserved on the difference mesh. For the case of non-periodic boundaries, this would correspond to placing the wall midway between the two end mesh points. There are circumstances where this is neither possible nor desirable, in which case separate difference methods must be used to advance the boundary points. Such methods will be discussed in Section 4.

The differential equation for the lth component of vector a conservation law appears as

$$\frac{\partial v^l}{\partial t} = -\frac{1}{h_1 h_2 h_3}\left[\frac{\partial}{\partial x_1}(h_2 h_3 T^{1,l}) + \frac{\partial}{\partial x_2}(h_1 h_3 T^{2,l})\right] + S^l, \tag{3.6}$$

where S^l represents the effective source of v^l due to the Coriolis terms. Again, using (3.4a) and (3.4b) we find the finite-difference approximation of (3.6) to be

$$\frac{\partial v_{ij}^l}{\partial t} = -\frac{2}{(h_1 h_2 h_3)_{ij}}\left[\frac{(h_2 h_3 T^{1,l})_{i+1/2,j} - (h_2 h_3 T^{1,l})_{i-1/2,j}}{\Delta_+ x_1 + \Delta_- x_1}\right.$$
$$\left. + \frac{(h_1 h_3 T^{2,l})_{i,j+1/2} - (h_1 h_3 T^{2,l})_{i,j-1/2}}{\Delta_+ x_2 + \Delta_- x_2}\right] + S_{i,j}^l. \tag{3.7}$$

To obtain a conservative difference approximation to a pseudovector conservation law

$$\frac{\partial \mathbf{w}}{\partial t} = \nabla \times \mathbf{G} \tag{3.8}$$

(e.g., (2.1a)), we must base our conservation sums on Stokes' theorem rather than the divergence theorem. Consider, for example, a small surface element lying in the $x_1 =$ constant plane (see Fig. 2). The center of this element has coordinates (x_1, x_2, x_3), and it has sides of length Δx_2 and Δx_3. The curve C forms the boundary of the element. Then integrating (3.8) over this surface element, applying Stokes' theorem, and using (3.4) results in the difference formula

$$\frac{\partial w_1}{\partial t} = \frac{1}{h_2 h_3 \Delta x_2}[(h_3 G_3)_{j+1/2} - (h_3 G_3)_{j-1/2}]$$
$$- \frac{1}{h_2 h_3 \Delta x_3}[(h_2 G_2)_{k+1/2} - (h_2 G_2)_{k-1/2}], \tag{3.9}$$

where the center of the surface element has indices (i, j, k) and we have suppressed nonvarying indices. The quantity to be conserved is now the flux through a surface of constant x_1 ($x_{2_{\min}} \leqslant x_2 \leqslant x_{2_{\max}}$, $x_{3_{\min}} \leqslant x_3 \leqslant x_{3_{\max}}$) consisting of many small elements such as the one just considered. We write this flux as

$$\Phi = \sum_{j,k} \phi_{i,j,k}. \tag{3.10}$$

The time derivative of this quantity is

$$\frac{\partial \Phi}{\partial t} = \sum_{j,k} \frac{\partial \phi}{\partial t} = \sum_{j,k} h_2 h_3 \Delta x_2 \Delta x_3 \frac{\partial w_1}{\partial t}. \tag{3.11}$$

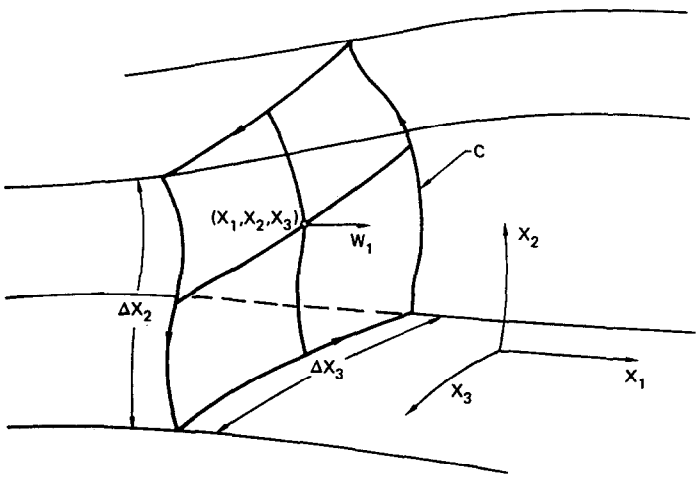

FIG. 2. Computational cell in the x_1-plane used for the derivation of the finite-difference approximation to pseudovector conservation laws.

Then using (3.14), we have

$$\frac{\partial \Phi}{\partial t} = \Delta x_3 \sum_k [(h_3 G_3)_{J-1/2} - (h_3 G_3)_{3/2}]$$

$$- \Delta x_2 \sum_j [(h_2 G_2)_{K-1/2} - (h_2 G_2)_{3/2}] \tag{3.12}$$

so that the rate of change of the total flux Φ is determined by the circulation of $\mathbf{G}$ about the boundaries of the domain. Note that if we have a system that is periodic in x_2 so that $(h_3 G_3)_{J-1/2} = (h_3 G_3)_{3/2}$, and is independent of x_3, then Φ is conserved identically on the difference mesh. Such is the case, for example, in cylindrical coordinates ($x_1 = r$, $x_2 = \theta$, $x_3 = z$) when there is no axial dependence. Then radial flux is conserved.

3.2. *Spatial Differenting*

The system of conservation laws (2.3) can be formally written as

$$\frac{\partial \mathbf{U}}{\partial t} = -\nabla \cdot \mathbf{F}, \tag{3.13}$$

where $\mathbf{U}$ is the eight-component vector

$$\mathbf{U} = [B_1, B_2, B_3, \rho V_1, \rho V_2, \rho V_3, \rho, u] \tag{3.14}$$

and $\nabla \cdot \mathbf{F}$ represents the right-hand side of (2.1). In orthogonal curvilinear coordinates, and ignoring Coriolis terms, (3.13) becomes

$$\frac{\partial \mathbf{U}}{\partial t} = -\frac{1}{h_1 h_2 h_3}\left[\frac{\partial}{\partial x_1}(h_1 h_3 \mathbf{F}_1) + \frac{\partial}{\partial x_2}(h_1 h_3 \mathbf{F}_2)\right], \tag{3.15}$$

where the $\mathbf{F}_i$ are eight-component vectors representing the fluxes of the components of $\mathbf{U}$. These have the general form

$$\mathbf{F}_i = \mathbf{A}_i \cdot \frac{\partial \mathbf{U}}{\partial x_1} + \mathbf{B}_i \cdot \frac{\partial \mathbf{U}}{\partial x_2} + \mathbf{C}_i \cdot \mathbf{U}, \tag{3.16}$$

where $\mathbf{A}_i$, $\mathbf{B}_i$, and $\mathbf{C}_i$ are 8×8 matrices which serve to couple the various components of (3.15). We see that there are first derivatives, second derivatives, and mixed derivatives appearing in these equations. We shall now describe the treatment of first and second derivatives. The treatment of mixed derivatives is more closely tied to the temporal differencing and will be discussed in the next section.

One result of the treatment of the conservation laws as given in Section 3.1 was to arrive at formulas for the spatial differencing of first derivatives of the fluxes. For example, we have for a nonuniform mesh

$$\frac{\partial F}{\partial x} = 2\frac{F_{j+1/2} - F_{j-1/2}}{\Delta_+ x + \Delta_- x}, \tag{3.17}$$

where we have used the identity

$$\tfrac{1}{2}(\Delta_+ x + \Delta_- x) = x_{j+1/2} - x_{j-1/2}.$$

The truncation error is

$$e_T = -\frac{1}{4}F''\frac{\Delta_+ x^2 - \Delta_- x^2}{\Delta_+ x + \Delta_- x} - \frac{1}{24}F'''\frac{\Delta_+ x^3 + \Delta_- x^3}{\Delta_+ x + \Delta_- x} \tag{3.18}$$

so that (3.17) is formally first-order accurate, becoming second order only on a uniform mesh. However, if the mesh spacing does not vary greatly from one mesh point to another, then the first term in (3.18) can be small, and effective second-order accuracy can by maintained. For example, in this work the mesh spacing is varied such that $\Delta_+ x/\Delta_- x = r$, where r is a constant differing only slightly from unity. Then (3.18) becomes

$$e_T = -\frac{1}{4}F''(r-1)\,\Delta_- x - \frac{1}{24}F'''\frac{r^3+1}{r+1}\Delta_- x^2.$$

If $r = 1 + \epsilon$, $\epsilon \approx O(\Delta_- x)$, effective second-order accuracy is achieved.

First derivatives appearing in F are differenced in a straightforward manner. We write

$$\frac{\partial}{\partial x}(af) = 2\frac{(af)_{j+1/2} - (af)_{j-1/2}}{\Delta_+ x + \Delta_- x}$$
$$= \frac{(af)_{j+1} - (af)_{j-1}}{\Delta_+ x + \Delta_- x}, \tag{3.19}$$

while second derivatives are differenced as

$$\frac{\partial}{\partial x}\left(a\frac{\partial f}{\partial x}\right) = \frac{2}{\Delta_+ x + \Delta_- x}\left[\left(a\frac{\partial f}{\partial x}\right)_{j+1/2} - \left(a\frac{\partial f}{\partial x}\right)_{j-1/2}\right]$$
$$= \frac{2}{\Delta_+ x + \Delta_- x}\left[a_{j+1/2}\frac{f_{j+1} - f_j}{\Delta_+ x} - a_{j-1/2}\frac{f_j - f_{j-1}}{\Delta_- x}\right], \tag{3.20}$$

which is again consistent with the basic formula (3.17).

3.3. *Temporal Differenting*

So far we have only dealt with spatial discretization, i.e., the replacement of spatial differential operators with spatial finite-difference operations. The equations we have derived have been of the form

$$\frac{\partial \mathbf{U}}{\partial t} = (D_1 + D_2 + D_{12})\mathbf{U}, \tag{3.21}$$

where D_1 represents first and second finite-difference operations in the x_1 direction, D_2 represents first and second finite-difference operations in the x_2 direction, D_{12} represents the (as yet unspecified) finite-difference approximation to the mixed derivatives, and $\mathbf{U}$ is a state vector of length M.

The size of the problem can be greatly reduced, and the desirable stability and accuracy properties maintained, by applying multistep temporal differencing methods. In this work, we use the Alternating Direction Implicit (ADI) [33, 34] scheme

$$\left(1 - \frac{\Delta t}{2}D_1\right)\mathbf{U}^{n+1/2} = \left(1 + \frac{\Delta t}{2}D_2\right)\mathbf{U}^n, \tag{3.22a}$$

$$\left(1 - \frac{\Delta t}{2}D_2\right)\mathbf{U}^{n+1} = \left(1 + \frac{\Delta t}{2}D_1\right)\mathbf{U}^{n+1/2}. \tag{3.22b}$$

The inclusion of mixed derivative terms in the equations presents special problems to which no satisfactory solution has been found. The difficulty lies in the fact that the operator D_{12} couples mesh points in both coordinate directions so that it does not

fit easily into the ADI scheme. This coupling is seen by a straightforward extension of (3.17). We have, for example,

$$\frac{\partial}{\partial x_2}\left(a\frac{\partial f}{\partial x_1}\right) = \frac{2}{\Delta_+ x_2 + \Delta_- x_2}\left[\left(a\frac{\partial f}{\partial x_1}\right)_{i,j+1/2} - \left(a\frac{\partial f}{\partial x_1}\right)_{i,j-1/2}\right]. \tag{3.23}$$

The terms $(a\,\partial f/\partial x_1)_{j\pm 1/2}$ are the fluxes at the top and bottom of the cell. It is clear that when the derivatives on the right-hand side are replaced by finite differences, neighboring points in both coordinate directions will be coupled. Marx [35] has used a scheme which allows splitting of this operator and still retains second-order accuracy, but this method is not conservative, since now the fluxes at the top and bottom of the cell appear at different time levels, and we cannot achieve the exact cell-to-cell cancellation of fluxes required for conservation.

Thus in choosing a scheme for the mixed derivative we must strike a compromise between second-order time accuracy and conservation (which is in itself a measure of accuracy). In this work we choose to retain conservation on the difference mesh by always treating the mixed derivatives explicitly (i.e., at the "old" time level). We use

$$\begin{aligned}\frac{\partial}{\partial x_1}\left(a\frac{\partial f}{\partial x_2}\right) = C[&a_{i+1/2,j}(f_{i+1,j+1} + f_{i,j+1} - f_{i+1,j-1} - f_{i,j-1}) \\ &- a_{i-1/2,j}(f_{i,j+1} + f_{i-1,j+1} - f_{i,j-1} - f_{i-1,j-1})]\end{aligned} \tag{3.24a}$$

and

$$\begin{aligned}\frac{\partial}{\partial x_2}\left(a\frac{\partial f}{\partial x_1}\right) = C[&a_{i,j+1/2}(f_{i+1,j+1} + f_{i+1,j} - f_{i-1,j+1} + f_{i-1,j}) \\ &- a_{i,j-1/2}(f_{i+1,j} + f_{i+1,j-1} - f_{i-1,j} - f_{i-1,j-1})],\end{aligned} \tag{3.24b}$$

where $C = (\Delta_+ x_1 + \Delta_- x_1)^{-1}(\Delta_+ x_2 + \Delta_- x_2)^{-1}$.

The Coriolis terms (see Eq. (3.6)) are time centered on each half time step, i.e.,

$$S_{i,j}^{(1)} = \tfrac{1}{2}(S_{i,j}^{n+1/2} + S_{i,j}^{n}),$$

$$S_{i,j}^{(2)} = \tfrac{1}{2}(S_{i,j}^{n+1} + S_{i,j}^{n+1/2})$$

so that the overall time centering of these terms is achieved.

The final set of difference equations can be written symbolically as

$$\left[1 - \frac{\Delta t}{2}(D_1 + S)\right]\mathbf{U}^{n+1/2} = \left[1 + \frac{\Delta t}{2}(D_2 + D_{12} + S)\right]\mathbf{U}^{n}, \tag{3.25a}$$

$$\left[1 - \frac{\Delta t}{2}(D_2 + S)\right]\mathbf{U}^{n+1} = \left[1 + \frac{\Delta t}{2}(D_1 + D_{12} + S)\right]\mathbf{U}^{n+1/2}, \tag{3.25b}$$

where the operator S represents the effect of the Coriolis terms, as described above.

3.4. *Solution of the Difference Equations*

Since the operators D_1, D_2, D_{12}, and S are in general nonlinear, each step of the ADI algorithm, Eqs. (3.25a) and (3.25b), represents a set of $M \times J$ (where M is the length of $\mathbf{U}$ and J is the number of mesh points in one direction) nonlinear algebraic equations to be solved on each row of the mesh. These equations must be linearized and solved iteratively. Lindemuth [19], and Finan [22], have used a multidimensional Newton–Raphson procedure to accomplish both linearizeation and solution. Here we use a more direct approach.

We consider the momenta, not the velocities, to be the dependent variables. The velocities are considered to be auxiliary variables and are calculated as momentum divided by density. They are always treated as coefficients. For example, in the equations for the time rate of change of the magnetic field, there appear terms V_iB_j. These terms are always written as

$$(V_iB_j)^{(l)} = V_i^{(l-1)}B_j^{(l)},$$

where the superscript (l) refers to the lth iteration of the solution of the nonlinear equations. The pressure is also considered an auxiliary variable, and is calculated at each iteration as

$$p^{(l)} = (\gamma - 1)[u^{(l)} - (\rho V^{(l)})^2/\rho^{(l)} - B^{(l)2}].$$

The pressure gradient terms are thus treated "explicitly" (i.e., considered as known quantities at the last iteration of the new time step). Terms which appear as products of unknowns are linearized as

$$(fg)^{(l)} = \tfrac{1}{2}(f^{(l-1)}g^{(l)} + g^{(l-1)}f^{(l)}),$$

where $f^{(l-1)}$ and $g^{(l-1)}$ are now considered as coefficients in the first and second terms, respectively. There are also terms which contain both products of unknowns and auxiliary variables. For example, one component of the Reynolds stress $\rho\mathbf{VV}$ is written as

$$\rho V_1V_2 = \tfrac{1}{2}[V_2^{(l-1)}(\rho V_1)^{(l)} + V_1^{(l-1)}(\rho V_2)^{(l)} + V_1^{(l-1)}V_2^{(l-1)}\rho^{(l)}].$$

Here, $V_2^{(l-1)}$, $V_1^{(l-1)}$, and $V_1^{(l-1)}V_2^{(l-1)}$ are treated as coefficients of the unknowns $(\rho V_1)^{(l)}$, $(\rho V_2)^{(l)}$, and $\rho^{(l)}$.

When Eqs. (3.25) are linearized in this manner, there results a set of simultaneous linear algebraic equations to be solved on each row of the mesh. Since the operators on the left-hand side of these equations couple at most three nearest neighbor points, the resulting system is block tridiagonal, and may be written in the form

$$-\mathbf{A}_{i,j}^{(l-1)} \cdot \mathbf{U}_{i+1,j}^{(l)} + \mathbf{B}_{i,j}^{(l-1)} \cdot \mathbf{U}_{i,j}^{(l)} - \mathbf{C}_{i,j}^{(l-1)} \cdot \mathbf{U}_{i-1,j}^{(l)} = \mathbf{D}_{i,j}, \qquad i = 2, 3, \ldots, I-1, \tag{3.26}$$

subject to the boundary condition

$$\mathbf{G}_1 \cdot \mathbf{U}_{1,j}^{(l)} = \mathbf{H}_1 \cdot \mathbf{U}_{2,j}^{(l)} + \mathbf{J}_1 \tag{3.27}$$

at the left-hand boundary, and

$$\mathbf{G}_I \cdot \mathbf{U}_{I,j}^{(l)} = \mathbf{H}_I \cdot \mathbf{U}_{I-1,j}^{(l)} + \mathbf{J}_I \tag{3.28}$$

at the right-hand boundary. Here **A**, **B**, **C**, **G**, and **H** are $M \times M$ matrices, $\mathbf{U}_{i,j}$ is the vector of length M of unknown quantities at the mesh point (i,j) $(1 \leqslant i \leqslant I, 1, \leqslant j \leqslant J)$, and **D** and **J** are vectors of length M. (Note that **A**, **B**, and **C** are not the same as those appearing in (3.16)). There is one equation for each interior mesh point on row j. For the model presented in Section 2, $M = 8$.

Equation (3.26), subject to (3.27) and (3.28), is solved by the well-known algorithm [36]

$$\mathbf{U}_{i,j}^{(l)} = \mathbf{E}_i \cdot \mathbf{U}_{i+1,j}^{(l)} + \mathbf{F}_i, \qquad i = I - 1, I - 2, \ldots, 1, \tag{3.29}$$

where $\mathbf{E}_i$ and $\mathbf{F}_i$ are defined recursively in terms of the boundary conditions. A similar solution can be defined when periodic boundary conditions are imposed [37]. In that case

$$\mathbf{U}_{i,j}^{(l)} = \mathbf{E}_i \cdot \mathbf{U}_{i+1,j}^{(l)} + \mathbf{S}_i \cdot \mathbf{U}_{I-1}^{(l)} + \mathbf{F}_i, \tag{3.30}$$

where **E**, **S**, and **F** are also determined recursively. Details of this method are presented in Appendix B.

Once the solution has been advanced to a new time level, the coefficients appearing in (3.26) are updated and the procedure is repeated until the solution converges to within a given tolerance. The time step is adjusted according to the number of iterations required for convergence [38]. If convergence cannot be achieved within a specified number of iterations, the time step is decreased. Conversely, if the solution converges rapidly, the time step is increased. Thus the code always uses the largest possible time step to maintain the desired accuracy. This iterative procedure is applied in a row by row manner. Since some rows converge faster than others, only limited regions of the mesh receive the maximum number of iterations; i.e., time is spent primarily in those regions where the solution is the most rapidly changing. It is thus impossible to give the exact number of iterations required for the entire mesh—one can only say that the most dynamic region of the system converges within the specified number of iterations (typically five). Using this method we generally run cases with time steps from 2 to more than 6 times larger than would be allowed by an explicit solution. The exact value depends on the desired accuracy.

4. Boundary Conditions

To advance a given magnetoplasma configuration forward in time, Eqs. (2.3) must be supplemented by boundary conditions. The case of periodic boundaries has been discussed in Section 3.4 and is detailed in Appendix B. In this section we discuss the conditions imposed at a conducting wall and at a singular ($r = 0$) boundary.

4.1. *Conducting Wall*

In inviscid flow, the primary boundary condition at a nonporous wall is

$$\hat{\mathbf{n}} \cdot \mathbf{V} = 0, \tag{4.1}$$

where $\hat{\mathbf{n}}$ is a unit vector normal to the wall and $\mathbf{V}$ is the velocity vector.

The boundary conditions on the electromagnetic field at a perfectly conducting wall are

$$\hat{\mathbf{n}} \cdot \mathbf{B} = 0, \tag{4.2}$$

$$\hat{\mathbf{n}} \times \mathbf{E} = 0; \tag{4.3}$$

i.e., the normal component of the magnetic field and the tangential component of the electric field must vanish. The first of these gives a condition on the normal component of $\mathbf{B}$, while the second can be used to derive conditions for the tangential components of $\mathbf{B}$. From Ohm's law and Ampère's law we have

$$(\eta/S)\nabla \times \mathbf{B} = \mathbf{E} + \mathbf{V} \times \mathbf{B}.$$

Taking $\hat{\mathbf{n}} \times$ this equation gives

$$(\eta/S)\hat{\mathbf{n}} \times (\nabla \times \mathbf{B}) = \hat{\mathbf{n}} \times \mathbf{E} + (\hat{\mathbf{n}} \cdot \mathbf{B})\mathbf{V} - (\hat{\mathbf{n}} \cdot \mathbf{V})\mathbf{B},$$

which, when evaluated at the wall, yields

$$\hat{\mathbf{n}} \times (\nabla \times \mathbf{B}) = 0. \tag{4.4}$$

Boundary conditions on the tangential components of velocity are found by requiring that, for inviscid flow, no vorticity be generated at the wall, i.e.,

$$\hat{\mathbf{n}} \times (\nabla \times \mathbf{V}) = 0. \tag{4.5}$$

We have found it convenient to impose boundary conditions on the thermodynamic variables ρ and u which require that mass and energy be conserved. We place the wall at $j = J$ and consider a half-sized cell extending from $j = J - \frac{1}{2}$ to $j = J$ (see Fig. 3), and we consider only the flux in the x_2 direction entering the cell. (We have here specified x_2 to be the coordinate normal to the wall.) If we define the "mass" in the interior cells (in one dimension) to be

$$M_{\text{INT}} = \sum_j \rho_j \Delta\tau_j = \frac{1}{2}\sum_j \rho_j h_1 h_2 h_3 (\Delta_+ x_2 + \Delta_- x_2), \tag{4.6}$$

where the sum extends over all cells up to $j = J - 1$, then the rate of change of this quantity is

$$\frac{\partial M_{\text{INT}}}{\partial t} = -(h_1 h_3 F_2)^{n+1}_{J-1/2}. \tag{4.7}$$

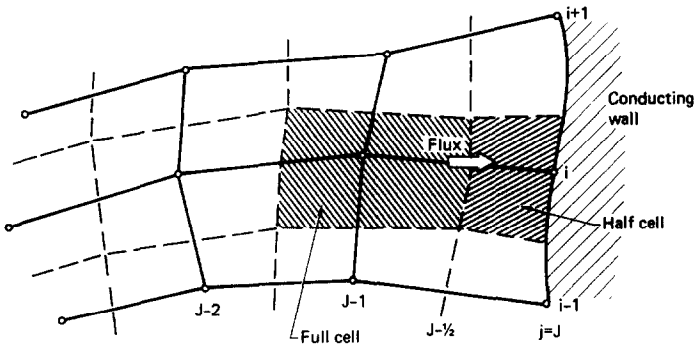

FIG. 3. Computational half-cell at solid boundary.

We now advance the boundary cell in such a way as to exactly cancel this change in mass on the interior of the mesh. We thus require

$$\frac{\partial \rho_J}{\partial t} \Delta\tau_J = (h_1 h_3 F_2)^{n+1}_{J-1/2} . \tag{4.8}$$

With

$$\Delta\tau_J = \tfrac{1}{2} h_1 h_2 h_3 \, \Delta_- x_{2_J} \tag{4.9}$$

as the volume of the boundary cell, we have

$$\frac{\partial \rho_J}{\partial t} = \frac{2}{(h_1 h_2 h_3)_J \, \Delta_- x_{2_J}} (h_1 h_3 F_2)^{n+1}_{J-1/2} \tag{4.10}$$

as the equation of the evolution of the density at the wall.

This procedure fits into our general boundary condition formulation. For example, the finite-difference approximation to the continuity equation (where $F_2 = \rho V_2$) is

$$-C(\rho v_2)^{n+1}_J + \rho^{n+1}_J = C(\rho v_2)^{n+1}_{J-1} + \rho_J{}^n \tag{4.11}$$

with

$$C = \frac{\Delta t (h_1 h_3)_{J-1/2}}{(h_1 h_2 h_3)_J (\Delta_- x_2)_J} .$$

The coefficients appearing in (4.11) become elements in the boundary condition matrices **G** and **H** (see Eqs. (3.27) and (3.28)).

4.2. *Singular Boundaries*

The problem of numerically advancing the solution at the origin of coordinates ($r = 0$) is a difficult one, for unless symmetry conditions exist there is no natural

boundary condition to be imposed at this point. This is because it is a boundary of the computational domain only by construction of the coordinate system. In this section we will present some special methods we have applied to this problem.

4.2.1. *Axial Symmetry* ($m = 0$)

For instabilities characterized by azimuthal mode number $m = 0$, we can pose the problem in (r, z) cylindrical coordinates. In this case, the solution at points on the axis $r = 0$ can be different for different values of z. This is in contrast to the case of polar or helical coordinates, where points on the axis for different values of the angular variable represent the same physical point in space.

From symmetry, we immediately have the boundary conditions

$$B_r = B_\theta = V_r = V_\theta = 0 \tag{4.12}$$

and

$$\frac{\partial B_z}{\partial r} = \frac{\partial V_z}{\partial r} = \frac{\partial \rho}{\partial r} = \frac{\partial u}{\partial r} \tag{4.13}$$

at $r = 0$. Equations (4.12) are easily implemented. However, if the boundary points of the mesh are to be placed on the axis (as they must be, since the coordinate system is not defined for negative r), Eqs. (4.13) become first-order accurate. To avoid this we apply a modification of the conservative boundary conditions described in Section 4.1 for these variables.

To illustrate this method, let us integrate the scalar conservation law

$$\frac{\partial u}{\partial t} = -\frac{1}{r}\frac{\partial}{\partial r}(rF) \tag{4.14}$$

over a cell which extends from $r = 0$ to $r = r_{3/2} = r_2/2$, where r_2 is the radius of the first interior mesh point. We find

$$\frac{\partial}{\partial t}\int_0^{r_{3/2}} ur\, dr = -\frac{1}{2} r_2 F_2 .$$

Then approximating the integral as

$$\int_0^{r_{3/2}} ur\, dr = \frac{1}{2} u_1 r_{3/2}^2$$

we arrive at

$$\frac{\partial u_1}{\partial t} = -\frac{4}{r_2} F_2 \tag{4.15}$$

as the equation for advancing u at the origin.

In this work we also include the axial fluxes in a straightforward manner. When this is done, we arrive at the following equations for advanding B_z, ρV_z, ρ, and u at the point $r = r_1 = 0$, $z = z_i$:

$$\frac{\partial B_{z_{i,1}}}{\partial t} = \frac{4}{r_2}\left\{(V_z B_r - V_r B_z)_{i,2} + \left[\frac{\eta}{S}\left(\frac{\partial B_z}{\partial r} - \frac{\partial B_r}{\partial z}\right)\right]_{i,3/2}\right\}, \tag{4.16a}$$

$$\frac{\partial(\rho V_z)_{i,1}}{\partial t} = -\frac{4}{r_2}(\rho V_r V_z - B_r B_z)_{i,2} - \frac{1}{\Delta_+ z + \Delta_- z}\left[\rho v_z^2 - B_z^2 + \frac{1}{2}(p + B_z^2)\right]\Big|_{i-1,1}^{i+1,1}, \tag{4.16b}$$

$$\frac{\partial \rho_{i,1}}{\partial t} = -\frac{4}{r_2}(\rho V_r)_{i,2} - \frac{1}{\Delta_+ z + \Delta_- z}(\rho V_z)\Big|_{i-1,1}^{i+1,1}, \tag{4.16c}$$

$$\frac{\partial u}{\partial t} = -\frac{4}{r_2}\left\{[(u + p - B_r^2 + B_\theta^2 + B_z^2) V_r - 2B_r(B_\theta V_\theta + B_z V_z)]_{i,2} - \frac{2\eta}{S}\left[rB_z\left(\frac{\partial B_z}{\partial r} - \frac{\partial B_r}{\partial z}\right) + B_\theta \frac{\partial}{\partial r}(rB_\theta)\right]_{i,3/2}\right\} - \frac{1}{(\Delta_+ z + \Delta_- z)}(u + p - B_z^2) V_z\Big|_{i-1,1}^{i+1,1}. \tag{4.16d}$$

In deriving these equations, we have made use of the boundary conditions (4.12).

4.2.2. *Scalar Quantities* ($m^2 > 0$)

In this and the following section we consider boundary conditions at the origin when there is no axial symmetry. In that case one of the independent variables is an angle (θ, say), and the origin represents the same point in space for all values of this coordinate.

Scalar quantities, such as ρ and u, must have unique values at the origin for any direction of approach; i.e., as we near the origin on any ray $\theta =$ constant, these quantities must approach the same limiting value. In polar and helical coordinates this is also the case for B_z and ρV_z. This comes about because the orientation of the unit vector in the z direction is independent of position. We advance such quantities at the origin by means of an algorithm which assures a solution which is consistent with that obtained on the interior of the mesh [39].

In helical coordinates (for example), a typical scalar conservation law is written

$$\frac{\partial u}{\partial t} = -\frac{1}{r}\frac{\partial}{\partial r}(rF) - \frac{1}{r}\frac{\partial G}{\partial \phi}, \tag{4.17}$$

where ϕ is defined in Eq. (2.5). Integration over a small cylindrical cell of radius $\Delta r/2$ yields

$$\frac{\partial u_0}{\partial t} = -\frac{2}{\pi \Delta r}\int_0^{2\pi} F\left(\frac{\Delta r}{2}, \phi\right) d\phi, \tag{4.18}$$

where u_0 is the value of u at $r = 0$, and the last term in (4.17) has vanished due to the assumed periodicity of G. On a finite-difference mesh, (4.18) becomes

$$\frac{\partial u_0}{\partial t} = \frac{-2}{\pi \Delta r} \sum_i \Delta\phi_i F_{i,3/2} \,. \tag{4.19}$$

As discussed in Section 3.4, the solution of the difference equations proceeds in partial time steps, so that on the partial step in which radial terms are treated explicitly, Eq. (4.19) can be used directly. On the other partial step F must be treated implicitly, thus coupling the solution for all rays (lines for which ϕ = constant) at the origin and seemingly destroying the well-known advantages of the ADI method. However, we will now show that this coupling can be used advantageously to obtain a self-consistent solution at the origin.

The radial flux F appearing in (4.19) will in general be nonlinear and will contain derivatives of u. After linearization and discretization, we can write

which, when substituted into (4.19), expresses u_0^{n+1} in terms of $u_{i,2}^{n+1}$ for all values of i, and displays the coupling of the rays discussed above. This coupling can be removed by modifying the recursive solution on the interior of the mesh. Instead of defining the solution as in (3.29), we write

$$u_{i,j}^{n+1} = e_{i,j} u_{i,j-1}^{n+1} + f_{i,j} \,, \qquad j = 2, 3, \ldots, J; \tag{4.21}$$

i.e., we define the solution from "left to right," instead of "right to left." Then using (4.20) and (4.21) in (4.19) yields

$$u_0^{n+1} = \left\{1 + \frac{\Delta t}{\pi \Delta r} \sum_i \Delta\phi_i (P_i e_{i,2} + Q_i)\right\}^{-1} \cdot \left\{u_0^n - \frac{\Delta t}{\pi \Delta r} \sum_i \Delta\phi_i (P_i f_{i,2} + R_i)\right\} \tag{4.22}$$

as the expression for the scalar u at the origin. The complete solution is thus obtained by sweeping *all* rays from the outer boundary to the origin to determine $e_{i,j}$ and $f_{i,j}$ recursively for $j = J - 1, J - 2, \ldots, 2$, applying (4.22), and then using (4.21) to obtain the interior solution.

4.2.3. *Symmetry Conditions* ($| m | > 1$)

At the origin, we know that the x and y (Cartesian) components of any vector quantity must be uniquely defined, whereas the r and θ components are not necessarily unique (i.e., they can have different values on each ray approaching the origin). Let $V_{r_{1,j}}$, $V_{\theta_{1,j}}$ be the r and θ components of a vector $\mathbf{V}$ at the origin for each value of

θ_j ($V_{r_{1,j}} = V_{r_1}(\theta_j)$, $V_{\theta_{1,j}} = V_{\theta_1}(\theta_j)$). We define the unique Cartesian components at the origin by the averaging procedure

$$\overline{V}_{x_1} = \frac{1}{2\pi}\int_0^{2\pi} [V_{r_1}(\theta)\cos\theta - V_{\theta_1}(\theta)\sin\theta]\,d\theta, \tag{4.23a}$$

$$\overline{V}_{y_1} = \frac{1}{2\pi}\int_0^{2\pi} [V_{r_1}(\theta)\sin\theta + V_{\theta_1}(\theta)\cos\theta]\,d\theta. \tag{4.23b}$$

But without loss of generality one of the components will vary like $\sin m\theta$, while the other will vary like $\cos m\theta$, so that

$$\overline{V}_{x_1} \approx \int_0^{2\pi} \left[\begin{Bmatrix}\sin m\theta\\ \cos m\theta\end{Bmatrix}\cos\theta - \begin{Bmatrix}\cos m\theta\\ \sin m\theta\end{Bmatrix}\sin\theta\right] d\theta, \tag{4.24a}$$

$$\overline{V}_{y_1} \approx \int_0^{2\pi} \left[\begin{Bmatrix}\\ \cos m\theta\end{Bmatrix}\sin\theta + \begin{Bmatrix}\cos m\theta\\ \sin m\theta\end{Bmatrix}\cos\theta\right] d\theta. \tag{4.24b}$$

Both of these vanish identically for $|\,m\,| > 1$. Then from

$$V_{r_{1,j}} = \overline{V}_{x_1}\cos\theta_j + \overline{V}_{y_1}\sin\theta_j\,, \tag{4.25a}$$

$$V_{\theta_{1,j}} = -\overline{V}_{x_1}\sin\theta_j + \overline{V}_{y_1}\cos\theta_j\,, \tag{4.25b}$$

we see that for these modes we have the symmetry condition that all vector components must vanish at the origin for each ray θ_j = constant.

4.2.4. *Vector Components* ($m = 1$)

When $m = 1$, the integrals in Eqs. (4.24) no longer vanish, so this mode is characterized by gross motion (e.g., nonvanishing velocity) across the origin. From (4.25), we see that the polar components of a vector need not be unique there. However, the Cartesian components must alwaus be unique, and we use this property to advance the vector components at $r = 0$.

The general form for the equation describing the evolution of a vector quantity is

$$\frac{\partial \mathbf{V}}{\partial t} = -\frac{1}{r}\frac{\partial}{\partial r}(r\mathbf{F}) - \frac{1}{r}\frac{\partial \mathbf{G}}{\partial \theta} - \frac{\partial \mathbf{H}}{\partial z} + \mathbf{C} + \nabla f, \tag{4.26}$$

where **F**, **G**, and **H** are the vector fluxes of **V**, and **C** represents possible Coriolis terms. We assume that the Cartesian representation of **V** can be obtained by the transformation

$$\mathbf{V}_c = \boldsymbol{\alpha}\cdot\mathbf{V}. \tag{4.27}$$

Then the Cartesian components of **V** evolve according to the equation

$$\frac{\partial \mathbf{V}_c}{\partial t} = -\frac{1}{r}\frac{\partial}{\partial r}(r\boldsymbol{\alpha}\cdot\mathbf{F}) - \frac{1}{r}\frac{\partial}{\partial\theta}(\boldsymbol{\alpha}\cdot G) - \frac{\partial}{\partial z}(\boldsymbol{\alpha}\cdot\mathbf{H}) + \frac{\partial\boldsymbol{\alpha}}{\partial z}\cdot\mathbf{H} + \boldsymbol{\alpha}\cdot\nabla f, \tag{4.28}$$

where we have assumed $\boldsymbol{\alpha}$ to be independent of r, and we have used

$$\boldsymbol{\alpha} \cdot \mathbf{C} = -\frac{1}{r}\frac{\partial \boldsymbol{\alpha}}{\partial \theta} \cdot \mathbf{G},$$

which, indeed, serves as a definition of the Coriolis term **C**.

When transformation to helical coordinates is performed, Eq. (4.28) becomes

$$\frac{\partial \mathbf{V}_c}{\partial t} = -\frac{1}{r}\frac{\partial}{\partial r}(r\boldsymbol{\alpha} \cdot \mathbf{F}) - \frac{1}{r}\frac{\partial}{\partial \phi}[\boldsymbol{\alpha} \cdot (\mathbf{G} + rk_z\mathbf{H})] + k_z \frac{\partial \boldsymbol{\alpha}}{\partial \theta} \cdot \mathbf{H} + \boldsymbol{\alpha} \cdot \nabla f, \quad (4.29)$$

which points out the reason for allowing $\boldsymbol{\alpha}$ to depend explicitly on the z coordinate.

Proceeding in a manner similar to that described in Section 4.2.2, we arrive at the equation

$$\frac{\partial \mathbf{V}_{c_0}}{\partial t} = -\frac{2}{\pi \Delta r}\int_0^{2\pi} d\theta \left[\boldsymbol{\alpha} \cdot \mathbf{F} - \frac{k_z \Delta r}{4}\frac{\partial \boldsymbol{\alpha}}{\partial \theta} \cdot \mathbf{H} + \frac{\Delta r}{4}\boldsymbol{\alpha} \cdot \nabla f\right]_{r=\Delta r/2} \quad (4.30)$$

for the evolution of the Cartesian components of **V** at the origin. In polar coordinates, the intergrand may be written as $\boldsymbol{\alpha} \cdot \mathbf{W}$, where

$$\mathbf{W} = \mathbf{F} - \frac{k_z \Delta r}{4}\mathbf{A} \cdot \mathbf{H} + \frac{\Delta r}{4}\nabla f.$$

Here we have used the fact that

$$\frac{\partial \boldsymbol{\alpha}}{\partial \theta} = \boldsymbol{\alpha} \cdot \mathbf{A},$$

where

$$\mathbf{A} = \begin{pmatrix} 0 & -1 \\ 1 & 0 \end{pmatrix}.$$

A self-consistent solution can now be defined in a manner analogous to that previously described for scalar variables. When we use the linearization

$$\mathbf{W}_{i,3/2}^{n+1} = \mathbf{P}_i \cdot \mathbf{V}_{i,2}^{n+1} + \mathbf{Q}_i \cdot \mathbf{V}_{c_0}^{n+1} + \mathbf{R}_i \quad (4.31)$$

we arrive at

$$\mathbf{V}_{c_0}^{n+1} = (\mathbf{I} + \mathbf{S})^{-1} \cdot (\mathbf{V}_{c_0}^{n} - \mathbf{T}), \quad (4.32)$$

where **I** is the identity matrix, and

$$\mathbf{S} = \frac{\Delta t}{\pi \Delta r}\sum_i \Delta\theta_i \boldsymbol{\alpha}_i \cdot [\mathbf{P}_i \cdot \mathbf{E}_{i,2} \cdot \boldsymbol{\alpha}_i^{-1} + \mathbf{Q}_i], \quad (4.33a)$$

$$\mathbf{T} = \frac{\Delta t}{\pi \Delta r}\sum_i \Delta\theta_i \boldsymbol{\alpha}_i \cdot [\mathbf{P}_i \cdot \mathbf{F}_{i,2} + \mathbf{R}_i]. \quad (4.33b)$$

The polar components are then obtained by inverting the transformation for each ray, and the interior solution is then found as described in Section 4.2.2.

5. APPLICATIONS

One of the features of the resistive MHD equations is the occurrence of phenomona which may evolve on widely separated time scales (see Section 2.1). Requirements of accuracy and stability on the numerical solutions of these equations require that such simulations evolve on the fast time scale. In that case, computational studies of events which evolve on the slow time scale become difficult whenever $S > O(1)$. Such is the case with resistive instabilities [23], which have no counterpart in ideal (infinitely conducting) MHD, and which grow on time scales which can approach the resistive diffusion time.

Recently certain of these resistive modes have been successfully studied [24–28] by employing a reduced set of equations [29] which, by assuming an ordering that eliminates the effects of plasma pressure, removes the fastest time scales from the problem and allows the numerical solution to proceed at a rapid rate. However, if one wishes to obtain solutions which may be applicable to such controlled fusion devices as High Beta Tokamaks and Reversed Field Pinches, the effects of plasma pressure must be included. Indeed, there exist resistive modes which appear only in the presence of finite pressure gradients [40]. Thus the numerical computation of resistive instabilities represents an important and extreme test of our model.

In addition, it is often desirable to perform calculations in several geometrical configurations. In many cases, one can best touch base with theory in slab geometry, while more realistic calculations require the use of other coordinate systems. Thus the ability to readily perform calculations in a variety of coordinate systems is extremely useful.

In this section we present sample calculations of resistive instabilities which demonstrate the performance of our model in light of the above discussion. For these examples we have taken $S \approx 10^{2-3}$, so that the time scales are well separated. We perform calculations in three different coordinate systems: Cartesian (x, y), axisymmetric cylindrical (r, z), and polar cylindrical (r, θ), and we present one example of the nonlinear evolution of a mode which appears only when the plasma possesses a finite pressure gradient.

5.1. *Slab Geometry*

We use Cartesian coordinates to study the tearing mode in a sheet pinch. The purpose of this study is twofold: (1) to serve as a check on the code by comparison with analytic results [23]; and (2) to display the nonlinear behavior of the mode.

We choose our equilibrium magnetic field configuration to be

$$B_x = \tanh(\pi/2)\, y,$$

which reverses direction at $y = 0$. We place conducting walls at $\pm y_w$ and assume a periodic structure in the x-direction. The scale length a in the y-direction is the half-width of the current sheet, while that in the x-direction is taken as the wavelength of

the perturbation. The resulting scale factors are $h_1 = 2\pi/\alpha$, $h_2 = h_3 = 1$, where $\alpha = ka$ is a nondimensional wavelength.

The perturbation quantities are the unstable eigenmodes obtained from a linear resistive MHD code [41]. These perturbation quantities, along with the equilibrium described above, constitute the initial conditions for the problem.

The growth rate of the resistive instability is determined by

$$p \equiv \omega t_H = \frac{1}{\Delta\phi} \frac{\partial \Delta\phi}{\partial t},$$

where $\Delta\phi = \phi_{\max} - \phi_{\min}$ and

$$\phi(x) = \int_{-y_w}^{0} B_x(0, y')\, dy' - \int_0^x B_y(x', 0)\, dx'$$

is the reconnected flux at the singular surface ($y = 0$).

When eigenfunctions of the linearized equations were introduced into the nonlinear code, the growth rate was found to be constant to four significant figures for 50 time steps. This value, as a function of S, was then compared with results obtained from the linear code (RIPPLE3) and those predicted by the linear analysis of [23], and are presented in Fig. 4. (The results obtained from the nonlinear code are labeled MHDG.) In studying these results it should be recalled that, in the present work, time is measured in units of the Alfvén transit time, while in [23] time is measured in units of the resistive diffusion time. Thus the usual formula $p \approx S^{2/5}$ must be converted to $p \approx S^{-3/5}$. This normalization more clearly displays the decrease in growth rate with decreasing resistivity (increasing S).

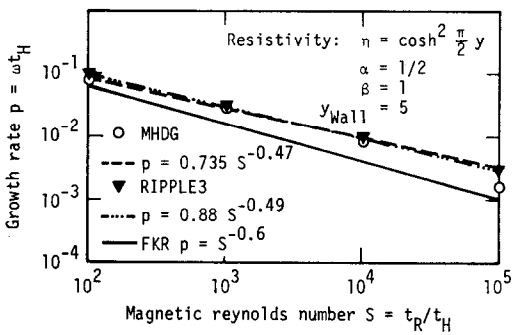

FIG. 4. Growth rate vs magnetic Reynolds number for the sheet pinch.

Two different models for resistivity were used: (1) an analytic model, $\eta = \cosh^2((\pi/2)\, y)$; and (2) Spitzer resistivity. The latter model is $\eta = T^{-3/2}$. Recalling that the temperature is peaked at $y = 0$, we see that for both models the resistivity is a minimum at the singular surface.

We find that the nonlinear code and the linear code agree quite well for low S ($<10^4$) and less well for higher S, for both resistivity models. For analytic resistivity we find a least-squares fit of the data over the range $10^2 \leqslant S \leqslant 10^5$ yields $p = 0.844S^{-0.494}$ for the linear code, and $p = 1.28S^{-0.559}$ for the nonlinear code. For a lower range of S, $10^2 \leqslant S \leqslant 10^4$, we find that the linear code yields $p = 0.792S^{-0.463}$ while the present model gives $p = 0.735S^{-0.473}$, demonstrating the close agreement between the two codes. These are to be compared with $p = 1.0S^{-0.6}$, the analytic result for this regime of [illegible]. For Spitzer resistivity a full range fit of the linear result [illegible] from the nonlinear code are $p = 1.23S$ [illegible] for the range of S, and $p = 0.734S^{-0.548}$ for low S. Thus, while the linear code, the nonlinear code, and theory agree quite well for low S, the present results actually agree better with theory over a larger range of magnetic Reynolds number.

Next the size of the perturbation and time step were increased and the mode was allowed to run into the nonlinear regime. The reconnected flux, $\Delta\phi_1$, as a function of time, for the case $S = 10^2$, is shown in Fig. 5. This mode was found to grow exponentially for some time and then begin to saturate. Figure 6 shows the magnetic flux surfaces after 10 Alfven transit times. This places it well into the nonlinear regime.

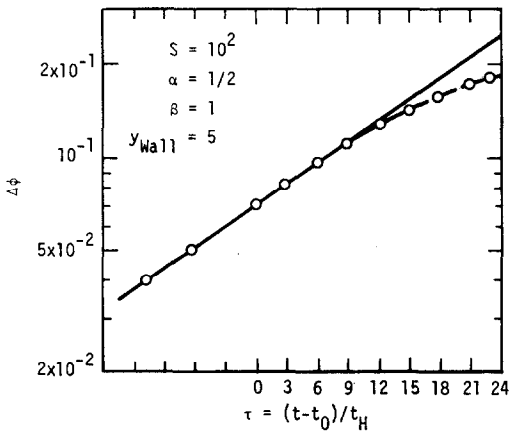

FIG. 5. Reconnected flux versus time for the sheet pinch.

The magnetic island is evident. It is seen that the nonlinear behavior of this mode does not cause drastic changes to the magnetic field structure away from the singular surface; i.e., the mode remains localized. However, since particles can easily stream along field lines, the change in topology has created a "short circuit" for particles to move from one side of the singular surface to the other, allowing for the possibility of an enhanced diffusion rate.

We have also used our model to study the nonlinear evolution of the double-tearing mode in this geometry [42].

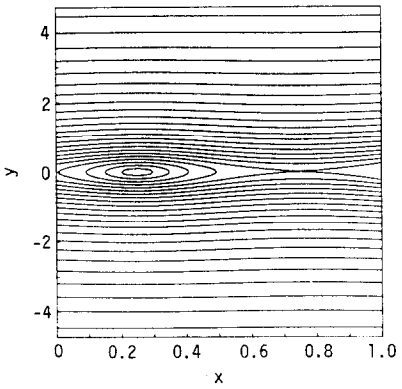

FIG. 6. Magnetic flux surfaces for the sheet pinch.

5.2. *Axial Symmetry* ($m = 0$)

Modes of a cylindrical plasma for which the azimuthal mode number m vanishes are axisymmetric because the perturbation no longer depends upon the angular variable θ. In this case the problem can be posed in (r, z) coordinates. In this section we present an example of a calculation performed in this coordinate system. For computational purposes, we take $x_1 = z$, $x_2 = r$, $x_3 = \theta$. The corresponding scale factors (see Section 2.2) are $h_1 = 2\pi/\alpha$, $h_2 = 1$, $h_3 = x_2$, where $\alpha = k_z a$ is the non-dimensional axial wave number. In addition to demonstrating the utility of posing the equations in orthogonal curvilinear coordinates, this case also serves as a test of the boundary conditions discussed in Section 4.2.2.

We consider an equilibrium in which the axial magnetic field B_z changes sign in the outer regions of the pinch. Such fields are characteristic of controlled fusion devices known as Reversed Field Pinches. Recently, analytic equilibria of this type have been discovered which are not only stable against tearing modes (resistive instabilities driven by the gross configuration of the magnetic field away from the singular ($\mathbf{k} \cdot \mathbf{B} = 0$) surface) at zero plasma $\beta(=p/B^2)$, but which are also stable against ideal interchange modes for values of β approaching 18 % [43]. However, these equilibria have been found to be unstable to slow resistive interchange modes [40], which are driven by the local pressure gradient at the singular surface. We perturb these equilibria with eigenfunctions obtained from a linear code [44], and follow the evolution of the mode into the nonlinear regime.

In Fig. 7 we show the initial flux surfaces for the case $S = 10^3$. The magnetic island due to the initial perturbation at the singular surface is present. In Fig. 8 we show the flux surfaces at $t = 595.5 t_H$, well into the nonlinear phase. Note the extreme distortion of the flux surfaces between the two large magnetic islands. The corresponding velocity field is shown in Fig. 9, and we note the localized interchange vortices in the region of largest flux surface distortion. The large radial extent of this flow pattern makes this mode particulary dangerous to plasma confinement.

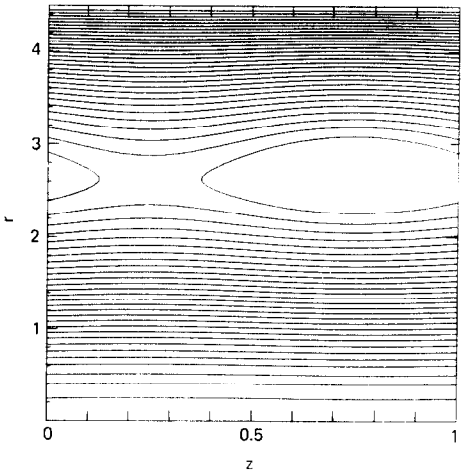

FIG. 7. Magnetic flux surfaces for resistive interchange mode, $m = 0$, $t = 0$.

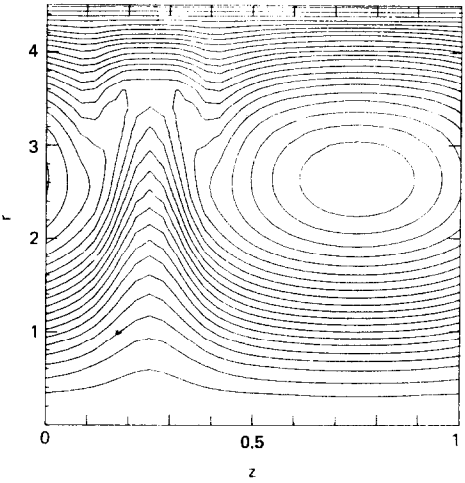

FIG. 8. Magnetic flux surfaces for resistive interchange mode, $m = 0$, $t = 595.5t_H$.

Note that this mode appears only when the plasma possesses a finite equilibrium pressure gradient (i.e., nonzero β). Such modes can only be studied by applying models which include these terms.

5.3. *Helical Symmetry* ($m > 0$)

As discussed in Section 2.3, modes for which both m and k_z are nonvanishing possess helical symmetry. The natural coordinate system for these calculations consists of a radial (r) and an angular (ϕ) variable. For such cases we take $x_1 = \phi$,

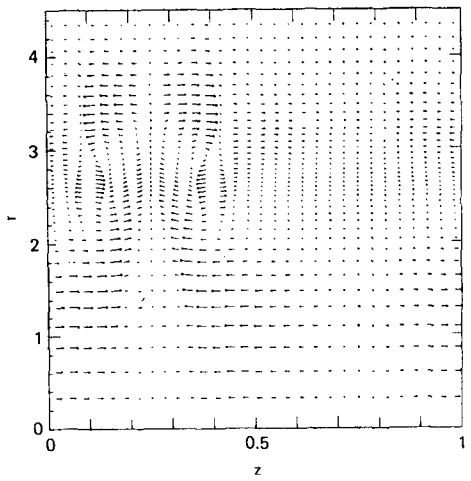

FIG. 9. Velocity field corresponding to Fig. 8.

$x_2 = r$, $x_3 = z$, $h_1 = x_2$, $h_2 = 1$, $h_3 = 1/\alpha$ and include the additional terms discussed in Section 2.3. These cases also require the use of the boundary conditions described in Sections 4.2.2–4.4. Thus, even though the physical geometry is still cylindrical. the computational geometry is entirely different from that described in Section 5.2, and again serves as a demonstration of the versatility of our model.

In these examples we consider the equilibrium given by

$$B_r = 0,$$
$$B_\theta = J_1(r),$$
$$B_z = J_0(r),$$

where J_0 and J_1 are the zero- and first-order Bessel functions. This equilibrium has the property of being force-free; i.e., the Lorentz force $\mathbf{J} \times \mathbf{B}$ vanishes identically. Thus no equilibrium pressure gradient exists, and we expect tearing modes to constitute the primary resistive instabilities. Also note that, for $r > 2.4$, the axial field reverses, so that this equilibrium can serve as a model of a Reversed Field Pinch.

For the case $m = 2$, we must use the boundary conditions discussed in Sections 4.2.2. and 4.2.3. In Fig. 10 we show the evolution of the flux surfaces for this mode for the case $S = 10^2$. We note that, after a short period of growth, saturation occurs at a level which leaves the overall plasma undisturbed. This mode remains localized in the same manner as discussed in Section 5.1. This behavior is summarized in Fig. 11, where we plot the exponential growth rate as a function of time. In this case, this quantity is determined by

$$p = \frac{1}{\Delta\psi_s} \frac{\partial \Delta\psi_s}{\partial t},$$

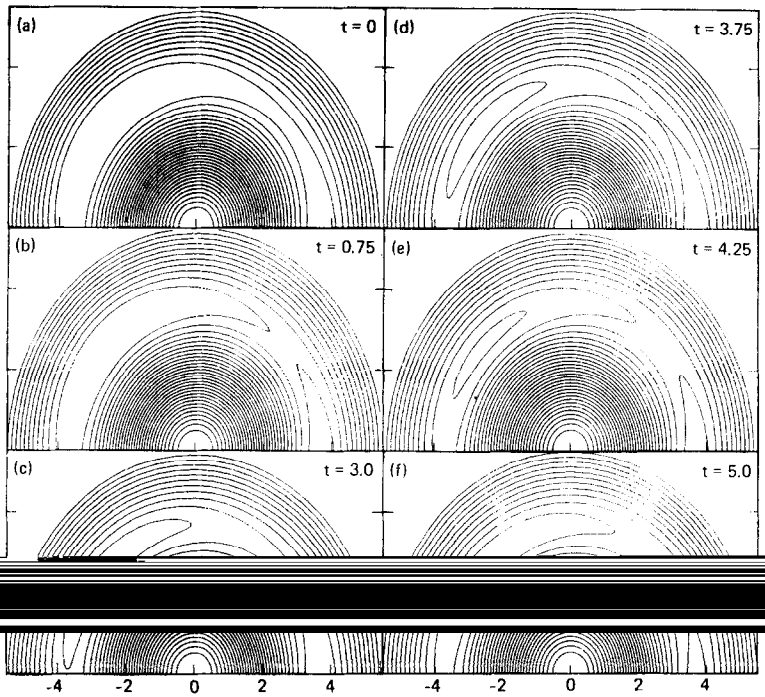

FIG. 10. Magnetic flux surfaces for the $m = 2$ mode in the Bessel function model.

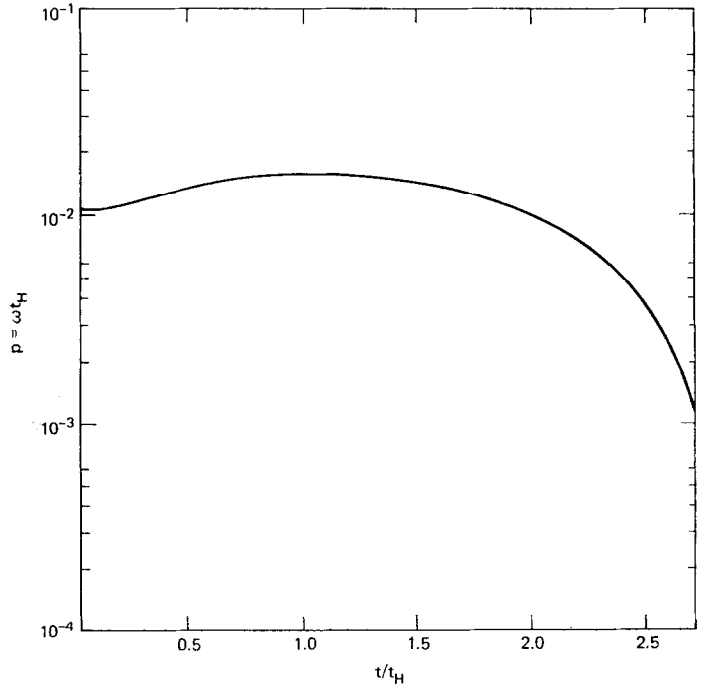

FIG. 11. Growth rate vs time for $m = 2$, Bessel function model.

where

$$\psi_s(\theta) = -\int_{(0,0)}^{(r_s,0)} (mB_\theta + rk_zB_z)_{\theta=0}\, dr + r_s \int_{(r_s,0)}^{(r_s,\theta)} B_r(r_s, \theta')\, d\theta'$$

is the helical flux, r_s is the radius of the singular surface, and $\Delta\psi_s = \psi_{s\,\max} - \psi_{s\,\min}$ is the reconnected helical flux. Note the initial exponential growth followed by rapid nonlinear saturation.

The case $m = 1$ is characterized by gross motion across the origin, so we must use the boundary conditions discussed in Section 4.2.4. In Fig. 12 we plot the reconnected

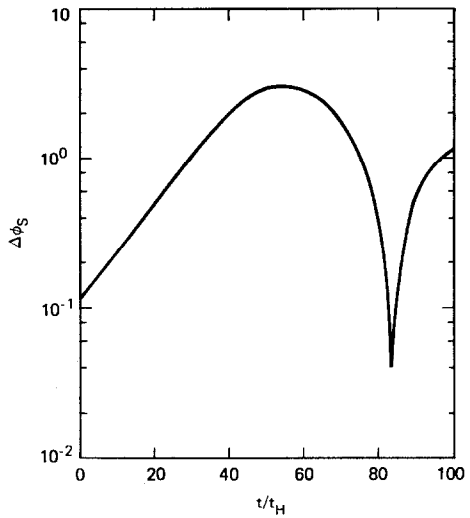

FIG. 12. Reconnected flux vs time for $m = 1$, Bessel function model.

helical flux as a function of time for this mode, again with $S = 10^2$. Note the extended period of exponential growth followed by complete nonlinear saturation. The evolution of the flux surfaces is shown in Fig. 13. For this mode we see that the magnetic island can grow to large size and, in the nonlinear phase, can occupy a considerable portion of the plasma volume. A more complete discussion of this behavior, which is qualitatively similar to that found for tokamak plasmas [29], can be found in Ref. [32]. Here we simply note that we have successfully simulated transport of both scalar and vector quantities across the origin by applying the methods described in Sections 4.2.2 and 4.2.4.

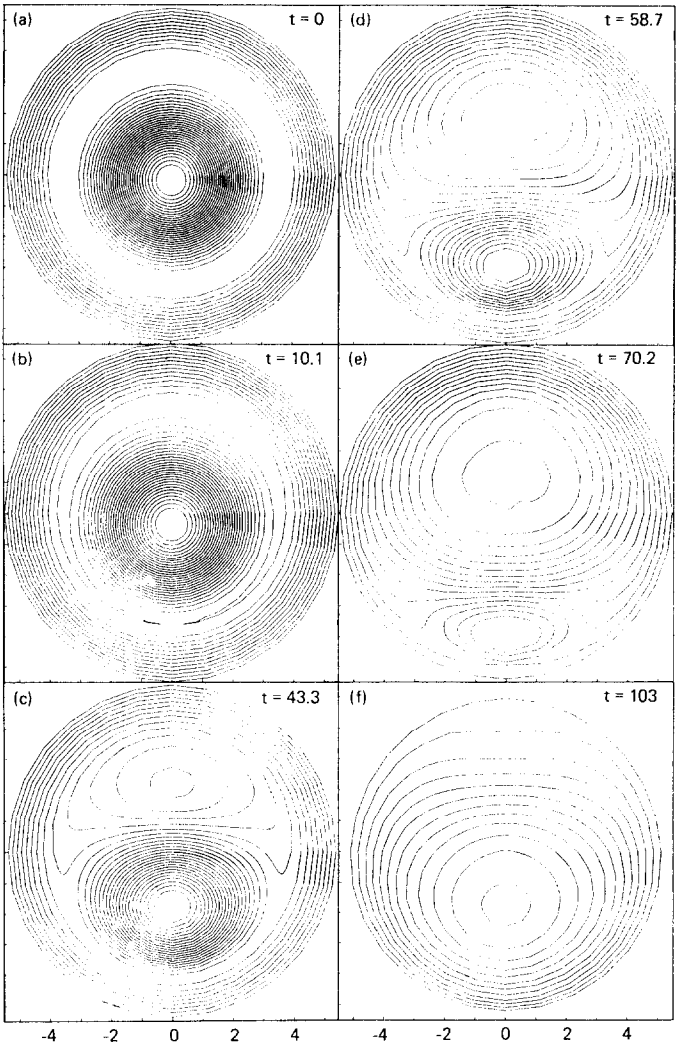

FIG. 13. Magnetic flux surfaces for the $m = 1$ mode in the Bessel function model.

6. SUMMARY

We have presented a computational model for the study of resistive magnetohydrodynamics. This model does not depend on assumptions about the ordering of various terms, and therefore contains all the macroscopic modes of a magnetoplasma system. It is unique in that it is applicable to a variety of coordinate systems.

We have developed numerical techniques for the solution of these equations. These techniques are based on an implicit treatment of the resulting difference equations,

and allow us to advance the solution at a rate several times faster than the fastest time scale in the problem. We have derived special boundary conditions for advancing the solution at a singular boundary, which must be accomplished if realistic simulations are to be performed.

We have presented examples of the application of our model to three distinct computational coordinate systems: Cartesian, axisymmetric, and polar. This effectively demonstrates the versatility of our approach. These examples involve the nonlinear evolution of resistive instabilities for cases in which the diffusive (slow) and convective (fast) time scales are well separated, and constitute an extreme test of our computational methods. The quantitative agreement with theoretical [23] results, and the qualitative agreement with previous numerical results [24], demonstrate the success of these techniques. In addition, we have presented results which depend critically on finite plasma pressure and cannot be obtained by the application of a reduced set of equations.

APPENDIX A. TWO-DIMENSIONAL MHD EQUATIONS IN ORTHOGONAL CURVILINEAR COORDINATES

In this Appendix we tabulate the two-dimensional resistive MHD equations which we solve in our code. They are obtained by expanding Eqs. (2.3). The result is

$$\frac{\partial B_1}{\partial t} = \frac{1}{h_2 h_3}\frac{\partial}{\partial x_2}\left\{h_3(V_1 B_2 - V_2 B_1) + \frac{1}{S}\frac{h_3\eta}{h_1 h_2}\left[\frac{\partial}{\partial x_2}(h_1 B_1) - \frac{\partial}{\partial x_1}(h_2 B_2)\right]\right\}, \tag{A1}$$

$$\frac{\partial B_2}{\partial t} = \frac{1}{h_1 h_3}\frac{\partial}{\partial x_1}\left\{h_3(V_2 B_1 - V_1 B_2) + \frac{1}{S}\frac{h_3\eta}{h_1 h_2}\left[\frac{\partial}{\partial x_1}(h_2 B_2) - \frac{\partial}{\partial x_2}(h_1 B_1)\right]\right\}, \tag{A2}$$

$$\frac{\partial B_3}{\partial t} = \frac{1}{h_1 h_2}\frac{\partial}{\partial x_1}\left\{h_2(V_3 B_1 - V_1 B_3) + \frac{1}{S}\frac{h_2\eta}{h_1 h_3}\frac{\partial}{\partial x_1}(h_3 B_3)\right\} + \frac{1}{h_1 h_2}\frac{\partial}{\partial x_2}\left\{h_1(V_3 B_2 - V_2 B_3) + \frac{1}{S}\frac{h_1\eta}{h_2 h_3}\frac{\partial}{\partial x_2}(h_3 B_3)\right\}, \tag{A3}$$

$$\frac{\partial(\rho V_1)}{\partial t} = -\frac{1}{h_1 h_2 h_3}\left\{\frac{\partial}{\partial x_1}[h_2 h_3(\rho V_1^2 - B_1^2)] + \frac{\partial}{\partial x_2}[h_1 h_3(\rho V_1 V_2 - B_1 B_2)] + h_3\frac{\partial h_1}{\partial x_2}(\rho V_1 V_2 - B_1 B_2) - h_3\frac{\partial h_2}{\partial x_1}(\rho V_2^2 - B_2^2) - h_2\frac{\partial h_3}{\partial x_1}(\rho V_3^2 - B_3^2)\right\} - \frac{1}{2}\frac{1}{h_1}\frac{\partial}{\partial x_1}(p + B^2), \tag{A4}$$

$$\frac{\partial(\rho V_2)}{\partial t} = -\frac{1}{h_1h_2h_3}\left\{\frac{\partial}{\partial x_1}[h_2h_3(\rho V_1V_2 - B_1B_2)] + \frac{\partial}{\partial x_2}[h_1h_3(\rho V_2{}^2 - B_2{}^2)]\right.$$
$$+ h_3\frac{\partial h_2}{\partial x_1}(\rho V_1V_2 - B_1B_2) - h_3\frac{\partial h_1}{\partial x_2}(\rho V_1{}^2 - B_1{}^2)$$
$$\left. - h_1\frac{\partial h_3}{\partial x_2}(\rho V_3{}^2 - B_3{}^2)\right\} - \frac{1}{2}\frac{1}{h_2}\frac{\partial}{\partial x_2}(p + B^2), \tag{A5}$$

$$\frac{\partial(\rho V_3)}{\partial t} = -\frac{1}{h_1h_2h_3}\left\{\frac{\partial}{\partial x_1}[h_2h_3(\rho V_1V_3 - B_1B_3)] + \frac{\partial}{\partial x_2}[h_1h_3(\rho V_2V_3 - B_2B_3)]\right.$$
$$\left. + h_2\frac{\partial h_3}{\partial x_1}(\rho V_1V_3 - B_1B_3) + h_1\frac{\partial h_3}{\partial x_2}(\rho V_2V_3 - B_2B_3)\right\}, \tag{A6}$$

$$\frac{\partial\rho}{\partial t} = -\frac{1}{h_1h_2h_3}\left\{\frac{\partial}{\partial x_1}(h_2h_3\rho V_1) + \frac{\partial}{\partial x_2}(h_1h_3\rho V_2)\right\}, \tag{A7}$$

and

$$\frac{\partial u}{\partial t} = -\frac{1}{h_1h_2h_3}\frac{\partial}{\partial x_1}\left\{h_2h_3\left[(u + p)\,V_1\right.\right.$$
$$- (B_1{}^2 - B_2{}^2 - B_3{}^2)\,V_1 - 2B_1(B_2V_2 + B_3B_3)$$
$$\left.\left. - \frac{2\eta}{S}\left\{\frac{B_3}{h_1h_3}\frac{\partial}{\partial x_1}(h_3B_3) + \frac{B_2}{h_1h_2}\left[\frac{\partial}{\partial x_1}(h_2B_2) - \frac{\partial}{\partial x_2}(h_1B_1)\right]\right\}\right]\right\}$$
$$- \frac{1}{h_1h_2h_3}\frac{\partial}{\partial x_2}\left\{h_1h_3\left[(u + p)\,V_2\right.\right.$$
$$+ (B_1{}^2 - B_2{}^2 + B_3{}^2)\,V_2 - 2B_2(B_1V_1 + B_3V_3)$$
$$\left.\left. + \frac{2\eta}{S}\left\{\frac{B_1}{h_1h_2}\left[\frac{\partial}{\partial x_1}(h_2B_2) - \frac{\partial}{\partial x_2}(h_1B_1)\right] - \frac{B_3}{h_2h_3}\frac{\partial}{\partial x_2}(h_3B_3)\right\}\right]\right\}. \tag{A8}$$

APPENDIX B. Solution of the Difference Equations with Periodic Boundary Conditions

In this Appendix we detail the solution of the difference equations

$$-\mathbf{A}_i\mathbf{U}_{i+1} + \mathbf{B}_i\mathbf{U}_i - \mathbf{C}_i\mathbf{U}_{i-1} = \mathbf{D}_i \tag{B1}$$

for $i = 2, 3, \ldots, I - 1$, subject to the periodic boundary conditions [37]

$$\mathbf{U}_1 = \mathbf{U}_{I-1}, \qquad \mathbf{U}_2 = \mathbf{U}_I. \tag{B2a, b}$$

These conditions are equivalent to requiring that $\mathbf{U}$ and its first derivative have the same value at $i = 3/2$ and $i = I - 1/2$.

Using these boundary conditions, we can write system (B1) as

$$\begin{aligned}
&\mathbf{B}_2 \cdot \mathbf{U}_2 - \mathbf{A}_2 \cdot \mathbf{U}_3 && - \mathbf{C}_2 \cdot \mathbf{U}_{I-1} = \mathbf{D}_2 \\
&\mathbf{C}_3 \cdot \mathbf{U}_2 + \mathbf{B}_3 \cdot \mathbf{U}_3 - \mathbf{A}_3 \cdot \mathbf{U}_4 && = \mathbf{D}_3 \\
&- \mathbf{C}_4 \cdot \mathbf{U}_3 + \mathbf{B}_4 \cdot \mathbf{U}_4 - \mathbf{A}_4 \cdot \mathbf{U}_5 && = \mathbf{D}_4 \\
&\qquad\vdots && \qquad\vdots \\
&\qquad - \mathbf{C}_{I-2} \cdot \mathbf{U}_{I-3} + \mathbf{B}_{I-2} \cdot \mathbf{U}_{I-2} - \mathbf{A}_{I-2} \cdot \mathbf{U}_{I-1} && = \mathbf{D}_{I-2} \\
&- \mathbf{A}_{I-1} \cdot \mathbf{U}_2 \qquad - \mathbf{C}_{I-1} \cdot \mathbf{U}_{I-2} + \mathbf{B}_{I-1} \cdot \mathbf{U}_{I-1} && = \mathbf{D}_{I-1}
\end{aligned} \tag{B3}$$

which comprise $I-2$ equations in the $I-2$ unknowns $\mathbf{U}_2, \mathbf{U}_3, \ldots, \mathbf{U}_{I-1}$. Except for the terms $-\mathbf{A}_{I-1} \cdot \mathbf{U}_2$ and $-\mathbf{C}_2 \cdot \mathbf{U}_{I-1}$, the system is block tridiagonal.

We now note that we could solve the first equation for $\mathbf{U}_2$ in terms of $\mathbf{U}_3$ and $\mathbf{U}_{I-1}$. We could then use this value of $\mathbf{U}_2$ to solve the second equation for $\mathbf{U}_3$ in terms of $\mathbf{U}_4$ and $\mathbf{U}_{I-1}$, and could continue on through the system, solving the $\mathbf{U}_i$ in terms of $\mathbf{U}_{i+1}$ and $\mathbf{U}_{I-1}$. We will thus seek a solution of the form

$$\mathbf{U}_i = \mathbf{E}_i \cdot \mathbf{U}_{i+1} + \mathbf{S}_i \cdot \mathbf{U}_{I-1} + \mathbf{F}_i . \tag{B4}$$

When this is used to eliminate $\mathbf{U}_{i-1}$ from (B1), we arrive at the recursion relations for **E**, **S**, and **F**. They are

$$\mathbf{E}_i = (\mathbf{B}_i - \mathbf{C}_i \cdot \mathbf{E}_{i-1})^{-1} \cdot \mathbf{A}_i , \tag{B5a}$$

$$\mathbf{S}_i = (\mathbf{B}_i - \mathbf{C}_i \cdot \mathbf{E}_{i-1})^{-1} \cdot \mathbf{C}_i \cdot \mathbf{S}_{i-1} , \tag{B5b}$$

$$\mathbf{F}_i = (\mathbf{B}_i - \mathbf{C}_i \cdot \mathbf{E}_{i-1})^{-1} \cdot (\mathbf{D}_i + \mathbf{C}_i \cdot \mathbf{F}_{i-1}). \tag{B5c}$$

From its construction, Eq. (B4) is equivalent to the ith equation of the set (B3). In particular, when applied to the $(I-2)$nd equation of the set, we arrive at an expression for $\mathbf{U}_{I-2}$ in terms of $\mathbf{U}_{I-1}$ only. This value could be used to eliminate $\mathbf{U}_{I-2}$ from the $(I-3)$rd equation, giving a value for $\mathbf{U}_{I-3}$ in terms of $\mathbf{U}_{I-1}$ only. This procedure could be continued through the rest of the equations. In general, for the ith equation, we would obtain relationship of the form

$$\mathbf{U}_i = \mathbf{T}_i \cdot \mathbf{U}_{I-1} + \mathbf{V}_i . \tag{B6}$$

Using this to eliminate $\mathbf{U}_{i+1}$ from (B4), we arrive at the recursion relations

$$\mathbf{T}_i = \mathbf{S}_i + \mathbf{E}_i \cdot \mathbf{T}_{i+1} , \tag{B7a}$$

$$\mathbf{V}_i = \mathbf{F}_i + \mathbf{E}_i \cdot \mathbf{V}_{i+1} . \tag{B7b}$$

We have now expressed all our unknows in terms of $\mathbf{U}_{I-1}$. To complete the solution, we apply (B1) at $i = I-1$, and use (B2b) and (B6). The result is

$$\begin{aligned}
\mathbf{U}_{I-1} = (&\mathbf{B}_{I-1} - \mathbf{A}_{I-1} \cdot \mathbf{T}_2 - \mathbf{C}_{I-1} \cdot \mathbf{T}_{I-2})^{-1} \cdot (\mathbf{D}_{I+1} \\
&+ \mathbf{A}_{I-1} \cdot \mathbf{V}_2 + \mathbf{C}_{I-1} \cdot \mathbf{V}_{I-2}).
\end{aligned} \tag{B8}$$

We now need starting conditions for the recursion relations (B5) and (B7). At $i = 1$ we have, from (B4),

$$\mathbf{U}_1 = \mathbf{E}_1 \cdot \mathbf{U}_2 + \mathbf{S}_1 \cdot \mathbf{U}_{I-1} + \mathbf{F}_1 .$$

This can be consistent with the boundary condition (B2a) only if

$$\mathbf{E}_1 = \boldsymbol{\phi}, \qquad \mathbf{F}_1 = \boldsymbol{\phi}, \qquad \mathbf{S}_1 = \mathbf{I}, \tag{B9}$$

where $\boldsymbol{\phi}$ is the zero matrix or vector, and $\mathbf{I}$ is the unit matrix. Using these, Eqs. (B5) define $\mathbf{E}$, $\mathbf{S}$, and $\mathbf{F}$ for $i = 2, 3, \ldots, I - 2$. Evaluating (B6) at $i = I - 1$, we conclude

$$\mathbf{T}_{I-1} = \mathbf{I}, \qquad \mathbf{V}_{I-1} = \boldsymbol{\phi}. \tag{B10}$$

These starting conditions, along with the $\mathbf{E}_i$, $\mathbf{S}_i$ and $\mathbf{F}_i$, can now be used in Eqs. (B7) to define $\mathbf{T}$ and $\mathbf{V}$, for $i = I-2, I-3, \ldots, 3, 2$. These values of $\mathbf{T}$ and $\mathbf{V}$, along with (B8), can then be used in Eqs. (B6) to solve for the $\mathbf{U}_i$ for $i = 2, 3, \ldots, I - 1$. The boundary conditions (B2) then define the remaining unknowns $\mathbf{U}_1$ and $\mathbf{U}_I$. Periodic boundary conditions thus require three sweeps of the mesh, whereas the regular boundary conditions (3.27) and (3.28) require only two.

ACKNOWLEDGMENTS

The authors wish to thank K. Marx and A. Mirin for many helpful discussions, and C. Finan for coding parts of the computer program and for providing his dynamic time step algorithm discussed in Section 3.4. One of us (D.S.) wishes to gratefully acknowledge H. R. Hicks and J. A. Holmes of Oak Ridge National Laboratory for an enlightening discussion of the treatment of scalar quantities at a singular boundary, as discussed in Section 4.2.2.

REFERENCES

1. R. C. GRIMM, J. M. GREENE, AND J. L. JOHNSON, *in* "Methods in Computational Physics" (J. Killeen, Ed.), Vol. 16, p. 253, Academic Press, New York, 1976.
2. K. APPERT, D. BERGER, R. GRUBER, AND J. RAPPAZ, *J. Comput. Phys.* **18** (1975), 284.
3. G. BATEMEN, W. SCHNEIDER, AND W. GROSSMANN, *Nucl. Fusion* **14** (1974), 669.
4. H. R. HICKS AND J. W. WOOTEN, *Comput. Phys. Comm.* **13** (1977), 117.
5. G. BATEMAN AND Y.-K. M. PENG, *Phys. Rev. Lett.* **38** (1977), 829.
6. J. DIBIASE AND J. KILLEEN, *J. Comput. Phys.* **24** (1977), 158.
7. K. V. ROBERTS AND D. E. POTTER, *in* "Methods in Computational Physics" (B. Alder, S. Fernbach and M. Rotenberg, Eds.), Vol. 9, p. 340, Academic Press, New York, 1970.
8. J. U. BRACKBILL, *in* "Methods in Computational Physics" (J. Killeen, Ed.), Vol. 16, p. 1, Academic Press, New York, 1976.
9. G. BATEMAN, H. R. HICKS, AND J. W. WOOTEN, *in* "Pulsed High Beta Plasmas" (D. E. Evans, Ed.), p. 557, Pergamon Press, Oxford, 1976.
10. S. C. JARDIN, J. L. JOHNSON, J. M. GREENE, AND R. C. GRIMM, *J. Comput. Phys.* **29** (1978), 101.

11. S. C. JARDIN AND J. L. JOHNSON, *in* "Proceedings, Eighth Conference on Numerical Simulation of Plasmas," paper OB-2, Monterey, Calif., 1978.
12. H. R. STRAUSS, *Phys. Fluids* **19** (1976), 134.
13. H. R. STRAUSS, *Phys. Fluids* **20** (1977), 1354.
14. J. A. WESSON AND A. SYKES, *in* "Proceedings, 5th Int. Cont. Tokyo, 1974," Vol. 1, p. 449, Intern. At. Energy Agency, Vienna, 1975.
15. G. BATEMAN *et al.*, *in* "Controlled Rusion and Plasma Physics" (Proc. 7th Europ. Conf., 1975), Vol. 1, p. 110, 1975.
16. A. SYKES AND J. A. WESSON, *Phys. Rev. Lett.* **37** (1976), 140.
17. F. L. COCHRAN, P. C. LIEWER, AND G. BATEMAN, *in* "Proceedings Eighth Conference on Numerical Simulation of Plasmas," paper PB-3, Monterey, Calif., 1978.
18. I. LINDEMUTH AND J. KILLEEN, *J. Comput. Phys.* **13** (1973), 181.
19. I. LINDEMUTH AND T. JARBOE, *Nucl. Fusion* **18** (1978), 929.
20. H. C. LUI AND C. K. CHU, *Phys. Fluids* **18** (1975), 1277.
21. H. C. LUI AND C. K. CHU, *Phys. Fluids* **19** (1976), 1947.
22. C. FINAN AND J. KILLEEN, *in* "Proceedings, Eighth Conference on Numerical Simulation of Plasmas," paper OA-3, Monterey, Calif., 1978.
23. H. P. FURTH, J. KILLEEN, AND M. N. ROSENBLUTH, *Phys. Fluids* **6** (1963), 459.
24. B. V. WADDELL, M. N. ROSENBLUTH, D. A. MONTICELLO, AND R. B. WHITE, *Nucl. Fusion* **16** (1976), 528.
25. H. R. HICKS, B. CARRERAS, J. A. HOLMES, AND B. V. WADDELL, ORNL/TM-60966 (1977).
26. B. V. WADDELL, B. CARRERAS, H. R. HICKS, J. A. HOLMES, AND D. K. LEE, ORNL/TM-6213 (1978).
27. B. CARRERAS, H. R. HICKS, AND B. V. WADDELL, ORNL/TM-6570 (1978).
28. G. L. JAHNS, M. SOLER, B. V. WADDELL, J. D. CALLEN, AND H. R. HICKS, *Nucl. Fusion* **18** (1978), 609.
29. M. N. ROSENBLUTH, D. A. MONTICELLO, H. R. STRAUSS, AND R. B. WHITE, *Phys. Fluids* **19** (1976), 1988.
30. P. M. MORSE AND H. FESHBACH, "Methods of Theoretical Physics," p. 47, McGraw–Hill, New York, 1953.
31. D. SCHNACK, Ph.D. thesis, University of California, Davis, UCRL-52399 (1978).
32. D. SCHNACK AND J. KILLEEN, *Nucl. Fusion* **19** (1979), 877.
33. D. W. PEACEMAN AND H. H. RACHFORD, JR., *SIAM J.* **3** (1955), 28.
34. J. DOUGLAS, *SIAM J.* **3** (1955), 42.
35. J. KILLEEN AND K. D. MARX, *in* "Methods in Computational Physics" (B. Alder, S. Fernbach, and M. Rotenberg, Eds.), Vol. 9, p. 422, Academic Press, New York, 1970.
36. R. D. RICHTMYER AND K. W. MORTON, "Difference Methods for Initial Value Problems," 2nd ed., Interscience, New York, 1967.
37. J. H. AHLBERG, E. N. NILSEN, AND J. L. WALSH, "Theory of Splines and Their Application," Academic Press, New York, 1967.
38. C. FINAN, private communication.
39. H. R. HICKS AND J. A. HOLMES, private communication.
40. B. COPPI, J. M. GREENE, AND J. L. JOHNSON, *Nucl. Fusion* **6** (1966), 101.
41. J. KILLEEN, *in* "Physics of Hot Plasmas" (B. J. Rye and J. C. Taylor, Eds.), p. 202, Plenum, New York, 1970.
42. D. SCHNACK AND J. KILLEEN, *in* "Theoretical and Computational Plasma Physics," p. 337, Intern. At. Energy Agency, Vienna, 1978.
43. D. C. ROBINSON, *Nucl. Fusion* **18** (1978), 939.
44. J. DIBIASE, Ph.D. thesis, University of California, Davis, UCRL-51591 (1974).
45. P. L. PRITCHETT, C. C. WU, AND J. M. DAWSON, *Phys. Fluids* **21** (1978), 1543.